Prepared for submission to JHEP

MPP-2012-125

Drastic Reduction of Cutoff Effects in 2-d Lattice $\mathrm{O}(N)$ Models

J. Balog,[a] **F. Niedermayer,**[b,c] **M. Pepe,**[d,b] **P. Weisz,**[e] **and U.-J. Wiese**[b]

[a] *Institute for Particle and Nuclear Physics, Wigner Research Centre for Physics, MTA Lendület Holographic QFT Group, 1525 Budapest 114, P.O.B. 49, Hungary*

[b] *Albert Einstein Center for Fundamental Physics Institute for Theoretical Physics, Bern University, Sidlerstr. 5, 3012 Bern, Switzerland*

[c] *Institute for Theoretical Physics – HAS, Eötvös University, Pázmány sétány 1/a, 1117 Budapest, Hungary*

[d] *INFN, Istituto Nazionale di Fisica Nucleare Sezione di Milano-Bicocca, Edificio U2, Piazza della Scienza 3 - 20126 Milano, Italy*

[e] *Max-Planck-Institut für Physik, 80805 Munich, Germany*

E-mail: balog.janos@wigner.mta.hu, niedermayer@itp.unibe.ch, Michele.Pepe@mib.infn.it, pew@mpp.mpg.de, wiese@itp.unibe.ch

Abstract: We investigate the cutoff effects in 2-d lattice O(N) models for a variety of lattice actions, and we identify a class of very simple actions for which the lattice artifacts are extremely small. One action agrees with the standard action, except that it constrains neighboring spins to a maximal relative angle δ. We fix δ by demanding that a particular value of the step scaling function agrees with its continuum result already on a rather coarse lattice. Remarkably, the cutoff effects of the entire step scaling function are then reduced to the per mille level. This also applies to the θ-vacuum effects of the step scaling function in the 2-d O(3) model. The cutoff effects of other physical observables including the renormalized coupling g_{R} and the mass in the isotensor channel are also reduced drastically. Another choice, the mixed action, which combines the standard quadratic with an appropriately tuned large quartic term, also has extremely small cutoff effects. The size of cutoff effects is also investigated analytically in 1-d and at $N = \infty$ in 2-d.

Contents

1 Introduction

2-d O(N) models share many features with 4-d non-Abelian gauge theories. They are asymptotically free, have a non-perturbatively generated mass gap, and, for $N = 3$, even instantons and θ-vacuum effects. 2-d O(N) models are integrable and have an analytically known exact S-matrix [1–3]. Based on this result, the exact mass gap has been extracted analytically [4]. This has even been extended to the mass gap $m(L)$ in a finite periodic volume of size L [5–8], which then provides exact information on the step scaling function introduced in [9]. Furthermore, O(N) models can be simulated very efficiently with the Wolff cluster algorithm [10, 11]. For these reasons, 2-d O(N) models are ideally suited as toy models for QCD, on which non-perturbative lattice methods can be tested with exquisite precision. Systematically controlling ultra-violet cutoff effects due to a finite lattice spacing a is a major objective of any lattice calculation. Symanzik's improvement program provides a reliable effective field theory basis for achieving this goal [12–15]. Interestingly, for many years the observed cutoff effects of the step scaling function in the 2-d O(3) model, which seemed to be of order $\mathcal{O}(a)$, were in apparent contradiction with the $\mathcal{O}(a^2)$ behavior predicted by Symanzik's theory [16]. Only recently, a careful higher-order investigation of Symanzik's effective theory resolved this puzzle by identifying large logarithmic corrections to the $\mathcal{O}(a^2)$ effects, which mimic $\mathcal{O}(a)$ behavior [18].

While Symanzik's improvement program aims at reducing cutoff effects in a systematic manner, order by order in the lattice spacing, the perfect action approach aims at completely eliminating cutoff effects at least at the classical level [19]. The fixed point action corresponding to a given renormalization group blocking transformation is indeed a classically perfect action, which is completely free of lattice spacing artifacts, even at arbitrarily coarse lattices. Remarkably, a practical parametrization of the classically perfect fixed point action, which includes a large number of terms beyond the standard nearest-neighbor coupling, was found to drastically reduce cutoff effects even at the quantum level [19]. Recently, the study of cutoff effects in the 2-d O(3) model has been driven to another extreme by studying topological actions [20]. Topological lattice actions are invariant against small continuous deformations of the lattice fields. The simplest topological action constrains the relative angle of neighboring O(N) spins to a maximally allowed angle δ, and assigns zero action to all allowed configurations. This action does not have the correct classical continuum limit, it cannot be studied in perturbation theory, and it violates the Schwarz inequality between action and topological charge for $N = 3$. Hence, one may consider this action as tree-level impaired (rather than e.g. 1-loop Symanzik improved). Despite these deficiencies, the 2-d O(3) model with a topological lattice action was still found to have the correct quantum continuum limit [20]. Its cutoff effects at practically accessible correlation lengths were found to be even smaller than those of the standard action. Interestingly, the topological lattice action approaches the continuum limit of the step scaling function from below, while the standard action approaches it from above.

In this paper, we combine the standard and the topological action to a non-topological constrained action. The relative angle between neighboring spins is again limited by a maximal angle δ, but allowed configurations are now assigned the standard action value.

Similar actions with a constraint have been used before in various contexts [21–34]. Here we optimize the constraint angle δ to reduce the cutoff effects in 2-d O(N) models. Remarkably, the cutoff effects of a variety of physical quantities including the step scaling function, the renormalized coupling $g_{\rm R}$, and the mass in the isotensor channel, as well as the vacuum angle θ-dependence of the mass gap for $N = 3$, turn out to be at most a few per mille, even on rather coarse lattices. This provides us with a very simple nearest-neighbor action that can be simulated very efficiently with the Wolff cluster algorithm [10, 11]. In fact, the optimized constrained action reduces cutoff effects at least to the same extent as the parametrized classically perfect action, but is a lot simpler. A mixed action, which combines the standard quadratic with a large quartic term suppresses cutoff effects equally well.

The paper is organized as follows. In section 2 we introduce the various actions to be considered in this work. Section 3 contains the investigation of the corresponding cutoff effects in the 2-d O(3) model first at vacuum angle $\theta = 0$, and then also at $\theta \neq 0$. In section 4, we study the 2-d O(4) and O(8) models in a similar manner, concentrating on the step-scaling functions. Section 5 addresses the cutoff effects in the $N = \infty$ limit analytically. Finally, Section 6 contains our conclusions. An analytic investigation of cutoff effects in the 1-d O(3) model is relegated to appendix A, while some technical details of the $N = \infty$ calculation are presented in appendix B.

2 Lattice Actions for O(N) Models

In this section we introduce various actions for O(N) models. In later sections we will compare the corresponding cutoff effects in order to identify a highly optimized lattice action. In the continuum, the action of the 2-d O(N) model is given by

$$S[\vec{e}] = \frac{1}{2g^2} \int \mathrm{d}^2x \; \partial_\mu \vec{e} \cdot \partial_\mu \vec{e}, \tag{2.1}$$

where $\vec{e}(x) = (e_1(x), e_2(x), \ldots, e_N(x))$ is an N-component unit-vector field, and g is the dimensionless coupling constant. Just as non-Abelian gauge theories in 4 space-time dimensions, 2-d O(N) models (with $N > 2$) are asymptotically free and have a non-perturbatively generated mass gap. For $N = 3$ one can define the topological charge

$$Q[\vec{e}] = \frac{1}{8\pi} \int \mathrm{d}^2x \; \varepsilon_{\mu\nu} \vec{e} \cdot (\partial_\mu \vec{e} \times \partial_\nu \vec{e}), \tag{2.2}$$

which is an element of the homotopy group $\Pi_2[S^2] = \mathbb{Z}$. In that case, one can introduce a vacuum angle θ and add $i\theta Q[\vec{e}]$ to the Euclidean action. Interestingly, as we have recently demonstrated, θ is a relevant parameter and there are distinct continuum theories for each value $\theta \in [0, \pi]$ [35]. This conclusion has been further supported by [36]. For $N > 3$, on the other hand, 2-d O(N) models are topologically trivial.

The standard action for the O(N) model on a 2-d square space-time lattice takes the form

$$S_{\rm std}[\vec{e}] = \beta \sum_{x,\mu} (1 - \vec{e}_x \cdot \vec{e}_{x+\hat{\mu}}), \tag{2.3}$$

where $\vec{e}_x$ is an N-component unit-vector associated with the lattice site x, and $\hat{\mu}$ points from x to the neighboring site $x+\hat{\mu}$ in the μ-direction. In the classical continuum limit the standard action with $\beta = 1/g^2$ reduces to the continuum action of eq. (2.1). According to Symanzik's effective theory, the standard action is expected to have cutoff effects of $\mathcal{O}(a^2)$. Recently, it has been observed that large logarithmic corrections, which also result from Symanzik's theory [18], can mimic the apparent $\mathcal{O}(a)$ behavior that was observed in numerical simulations [16, 17].

Recently, we have performed detailed investigations of so-called topological lattice actions [20], which are invariant against small deformations of the lattice field. Here we investigate a topological action that constrains the angle between neighboring spins by a maximal value δ. The topological action vanishes, i.e. $S_{\mathrm{top}}[\vec{e}] = 0$, if the constraint is satisfied for all nearest-neighbor spin pairs, i.e. $\vec{e}_x \cdot \vec{e}_{x+\hat{\mu}} > \cos\delta$, and is infinite otherwise. This action has already been considered earlier in [22–24, 26, 30], without emphasizing its topological features. Since the topological action vanishes for all allowed configurations, it has no meaningful classical continuum limit and cannot be treated in perturbation theory. Still, when one sends $\delta \to 0$, one approaches the correct quantum continuum limit [20, 26], which demonstrates that universality does not rely on the classical continuum limit. Interestingly, for the topological action the sign of the cutoff effects of some observables is opposite to the one resulting from the standard action.

In [35] we have used this observation to construct an optimized action with extremely small cutoff effects. The resulting constrained action combines the standard and the topological action such that

$$S_{\mathrm{con}}[\vec{e}] = \sum_{x,\mu} s(\vec{e}_x, \vec{e}_{x+\hat{\mu}}), \tag{2.4}$$

with

$$s(\vec{e}_x, \vec{e}_{x+\hat{\mu}}) = \beta(1 - \vec{e}_x \cdot \vec{e}_{x+\hat{\mu}}) \qquad \text{for} \quad \vec{e}_x \cdot \vec{e}_{x+\hat{\mu}} > \cos\delta, \tag{2.5}$$

and $s(\vec{e}_x, \vec{e}_{x+\hat{\mu}}) = \infty$ otherwise. For $\delta = \pi$ the constrained action reduces to the standard action, while for $\beta = 0$ it turns into the topological action. By optimizing the constraint angle to the value $\cos\delta = -0.345$, we have been able to reduce the cutoff effects below the per mille level in an investigation of lattice θ-vacua in the 2-d O(3) model [35]. When δ takes the optimized value, the constrained action $S_{\mathrm{con}}[\vec{e}]$ turns into the optimized constrained action $S_{\mathrm{oca}}[\vec{e}]$. In this paper, we construct such actions also for $N \neq 3$.

Finally, we consider the following quadratic plus quartic mixed action

$$S_{\mathrm{mix}}[\vec{e}] = \sum_{x,\mu} \left[\beta(1 - \vec{e}_x \cdot \vec{e}_{x+\hat{\mu}}) + \gamma(1 - \vec{e}_x \cdot \vec{e}_{x+\hat{\mu}})^2\right]. \tag{2.6}$$

For given β, we will adjust γ to reduce the cutoff effects, thus optimizing the action. When $\gamma \gtrsim \beta^2$ the mixed action can again not be treated in perturbation theory. When γ takes the optimized value, the mixed action $S_{\mathrm{mix}}[\vec{e}]$ turns into the optimized mixed action $S_{\mathrm{oma}}[\vec{e}]$.

Berg and Lüscher have introduced a geometric definition of the lattice topological charge [39]. In this definition, each lattice plaquette is divided into two triangles, as illustrated in figure 1. The spins $\vec{e}_x$, $\vec{e}_y$, and $\vec{e}_z$ at the three corners of a lattice triangle t_{xyz}

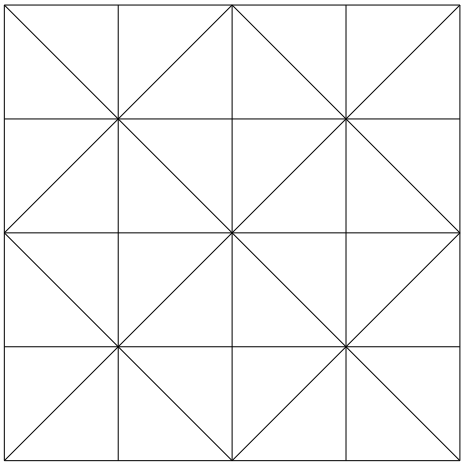

Figure 1. *Decomposition of the square lattice into triangles t_{xyz}. The topological charge density $A_{xyz}/4\pi$ of the 2-d lattice* O(3) *model is given by the oriented area A_{xyz} of the spherical triangle defined by the three spins $\vec{e}_x$, $\vec{e}_y$, and $\vec{e}_z$ at the corners of t_{xyz}.*

define the corners of a spherical triangle on S^2. The oriented area A_{xyz} of the spherical triangle is given by

$$\begin{aligned} &A_{xyz} = 2\varphi \in (-2\pi, 2\pi], \quad X + iY = r\exp(i\varphi), \\ &X = 1 + \vec{e}_x \cdot \vec{e}_y + \vec{e}_y \cdot \vec{e}_z + \vec{e}_z \cdot \vec{e}_x, \quad Y = \vec{e}_x \cdot (\vec{e}_y \times \vec{e}_z). \end{aligned} \tag{2.7}$$

The lattice topological charge is defined as the sum of the oriented areas A_{xyz} over all triangles t_{xyz}, normalized by the total area 4π of the sphere S^2, i.e.

$$Q[\vec{e}] = \frac{1}{4\pi} \sum_{t_{xyz}} A_{xyz} \in \mathbb{Z}. \tag{2.8}$$

The decomposition of the square lattice into triangles illustrated in figure 1 is invariant under 90 degrees rotations and under translations by an even number of lattice spacings. When a configuration is shifted by just one lattice spacing, the lattice plaquettes are divided into two triangles in a different manner than before, and thus the topological charge may change. However, this does not happen for sufficiently smooth configurations. In particular, one can show that a nearest-neighbor constraint angle $\delta < \pi/2$ (as used in the action S_{con}) leads to a completely translation invariant topological charge. In that case, just as in the continuum, different topological sectors are separated by infinite-action barriers.

3 Numerical Study of Cutoff Effects in the 2-d O(3) Model

In this section we investigate the cutoff effects of a variety of physical quantities. In particular, we address the question to what extent an action that was optimized to reproduce the continuum limit of a particular quantity automatically improves the scaling behavior of other observables.

3.1 The step scaling function at $\theta = 0$

The dimensionless physical quantity

$$u = Lm(L) = L/\xi(L), \tag{3.1}$$

is defined as the ratio of the spatial size L and the finite-volume correlation length $\xi(L) = 1/m(L)$. Based on this, one defines the step scaling function (with scale factor s) [9]

$$\sigma(s, u) = sLm(sL), \tag{3.2}$$

which is also known analytically [5]. By measuring the mass gaps $m(L)$ and $m(sL)$ in a Monte Carlo simulation on a lattice with L/a points in the periodic spatial direction, one obtains the lattice step scaling function $\Sigma(s, u, a/L) = sLm(sL, a/L)$.

Figure 2 compares the cutoff effects of $\Sigma(2, u_0, a/L)$ at $u_0 = 1.0595$ for five different lattice actions. While the standard action and the actions $D(1/3)$ and $D(-1/4)$ [40] (which contain additional diagonal neighbor couplings), approach the continuum limit from above, the topological action approaches it from below. By optimizing the constraint angle δ such that $\Sigma(2, u_0, a/L = 1/10)$ assumes its continuum value $\sigma(2, u_0) = 1.26121035$, one obtains $\cos\delta = -0.345$. The resulting optimized constrained action has extremely small cutoff effects in the per mille range also at other (not too coarse) values of the lattice spacing. Based on the analytic results of [40] the lattice data have been fitted to the expression

$$\Sigma(2, u, a/L) = \sigma(2, u) + \frac{a^2}{L^2}\left[B\log^3(L/a) + C\log^2(L/a) + \dots\right], \tag{3.3}$$

which gives good agreement with the analytically known continuum result. The above analytic form is justified theoretically for the standard action as well as for the actions $D(1/3)$ and $D(-1/4)$. Although, strictly speaking, it may no longer be justified to use the expression of eq. (3.3) to fit the topological action data, one again obtains excellent agreement with the continuum result. Interestingly, in the range of correlation lengths considered here, the lattice artifacts of the topological action are smaller than those of the standard action. In fact, for the standard action at $L/a = 64$ the sub-leading term proportional to $\log^2(L/a)$ is still larger than the leading term proportional to $\log^3(L/a)$, while this is not the case for the topological action [20]. Based on the fitted values of B and C, the lattice artifacts of the standard action are smaller than the ones of the topological action only for correlation lengths larger than about $5\times10^4 a$. Without re-adjusting δ, using the optimized constrained action (which was optimized for $u_0 = 1.0595$ at $L/a = 10$), the cutoff effects of the step scaling function are extremely small also for other values of u. Of course, one could also re-adjust δ for each value of L/a (always optimizing at u_0). Interestingly, the optimal value of δ is rather insensitive to L/a (as long as L/a is not too small).

Let us also pursue this more elaborate alternative optimization strategy, however, now applied to the mixed action. For each value of β, the parameter γ of the mixed action has been optimized to reproduce the analytically known continuum limit of the step 2 scaling function, i.e. $\Sigma(2, u_0, a/L) = \sigma(2, u_0) = 1.26121035$. The optimal values of β and γ are shown in figure 3 for various lattice sizes L/a. They are also listed in table 1.

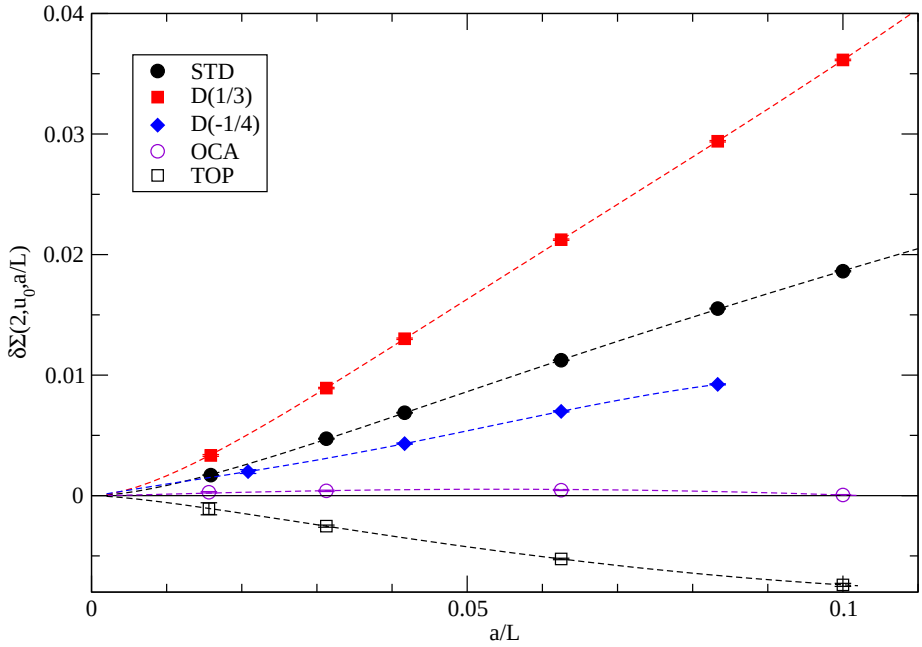

Figure 2. *Cutoff dependence of the step scaling function* $\Sigma(2, u_0, a/L)$ *for five different lattice actions: the standard action, the actions* $D(1/3)$ *and* $D(-1/4)$ *with additional diagonal neighbor couplings, the topological lattice action of [20], and the optimized constrained action with* $\cos\delta = -0.345$. *The lines for the standard action are fits based on eq. (3.3) . The horizontal line represents the analytic continuum result of [5].*

L/a	β	γ	u	$\Sigma(2, u, a/L)$	$\Sigma(2, u_0, a/L) - \sigma(2, u_0)$
10	0.31664	1.18790	1.059500(6)	1.261218(12)	0.000008(16)
16	0.51378	1.13480	1.059506(9)	1.261204(12)	−0.000016(19)
32	0.73962	1.10276	1.059505(9)	1.261167(17)	−0.000011(22)
64	0.95450	1.06820	1.059501(15)	1.261205(36)	−0.000007(44)

Table 1. *Optimized parameters* β *and* γ *for the mixed action such that* $\Sigma(2, u_0, a/L) = \sigma(2, u_0) = 1.26121035$. *The resulting value of* u *is very close to the desired* $u_0 = 1.0595$, *and* $\Sigma(2, u, a/L)$ *deviates very little from the continuum value* $\sigma(2, u_0)$. *The last column is the deviation of* $\Sigma(2, u_0, a/L)$ *(obtained by extrapolation from* u *to* u_0*) from the analytic result.*

Using the couplings of table 1, figure 4 shows the resulting cutoff effects of the step 3 scaling function $\Sigma(3, u_0, a/L)$ compared to the analytically known continuum result $\sigma(3, u_0) = 1.439574$. Without any further adjustable parameters, the mixed action optimized in this way automatically leads to a drastic reduction of the cutoff effects of $\Sigma(3, u_0, a/L)$.

3.2 The step scaling function at $\theta \neq 0$

While analytic results from the exact S-matrix exist only for $\theta = 0$ and $\theta = \pi$, the step scaling function is well-defined for all values of the vacuum angle θ. In [35] the step 2 scaling function has been determined at $\theta = 0, \pi/2$, and π. In this way, the conjectured

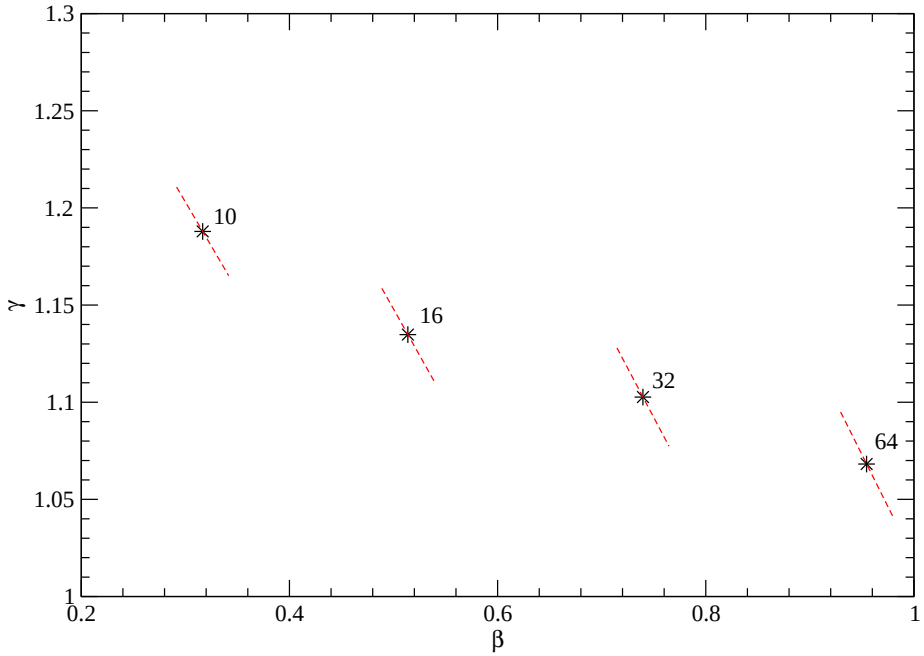

Figure 3. *Optimized parameters β and γ for the mixed action such that $\Sigma(2, u_0, a/L) = \sigma(2, u_0) =$ 1.26121035. The dashed lines represent the tangents to lines of constant $\Sigma(2, u_0, a/L)$, which are obtained by measuring the derivatives $\partial u/\partial\beta$ and $\partial u/\partial\gamma$.*

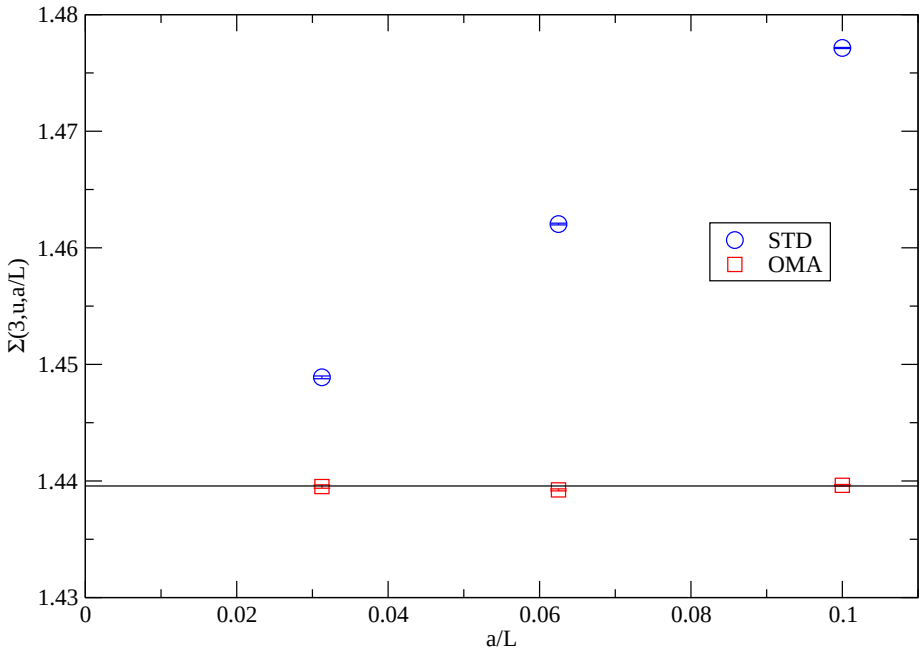

Figure 4. *Cutoff dependence of the step 3 scaling function $\Sigma(3, u_0, a/L)$ for the standard action and the optimized mixed action.*

exact S-matrix has been indirectly verified with per mille level accuracy. It also has been shown that the step scaling function at $\theta = \pi/2$ differs from the one at $\theta = 0$ and π.

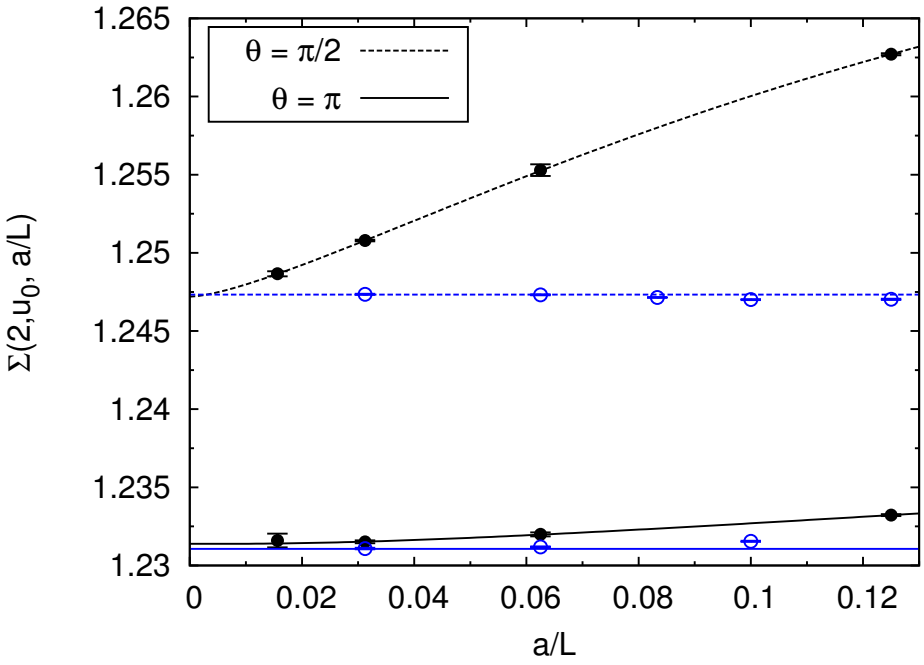

Figure 5. *Cutoff dependence of the step scaling function* $\Sigma(\theta, 2, u_0, a/L)$ *(with* $Lm(\theta, L) = u_0 = 1.0595$*) for the standard and for the optimized constrained action with* $\cos\delta = -0.345$*, at* $\theta = \pi/2$ *and* $\theta = \pi$*. The lines for the standard action are fits based on eq. (3.3). The horizontal lines represent the analytic result of [41] at* $\theta = \pi$*, and the fitted continuum value for* $\theta = \pi/2$*.*

This shows that θ does not get renormalized non-perturbatively and it indicates that all values of $\theta \in [0, \pi]$ are associated with distinct theories in the continuum limit. In view of the potentially devastating cutoff effects caused by dislocations, this is a non-trivial and somewhat unexpected result. Note, however, that a non-trivial θ-dependent spectrum is predicted by form-factor perturbation theory [37]. The spectrum was investigated by lattice Monte Carlo methods [38] using an imaginary θ and analytic continuation.

Figure 5, which is taken from [35], shows that without any further adjustments of δ, the cutoff effects of the optimized constrained action are automatically drastically reduced also at $\theta = \pi/2$ and π. The analytic result is known [41] for $\theta = \pi$ to be $\sigma(\pi, 2, u_0) = 1.231064$ for $u_0 = 1.0595$.

We have also considered $Lm(\theta, L)$ at fixed $Lm(0, L) = u_0 = 1.0595$, which is yet another physical quantity. Figure 6 illustrates the cutoff effects of the mass gap at $\theta = \pi$ for the optimized constrained action (with $cos\delta = -0.345$), the optimized mixed action and the standard action. Although the cutoff effects are only in the per mille range for the optimized actions, the approach to the continuum limit is non-uniform since the lattice results undershoot the exact continuum value before they ultimately approach it from below.

We have also measured $Lm(\pi/2, L)$ at fixed $Lm(0, L) = u_0 = 1.0595$ using the optimized mixed action with the couplings listed in table 1. As shown in figure 7, the cutoff effects are again drastically smaller than for the standard action.

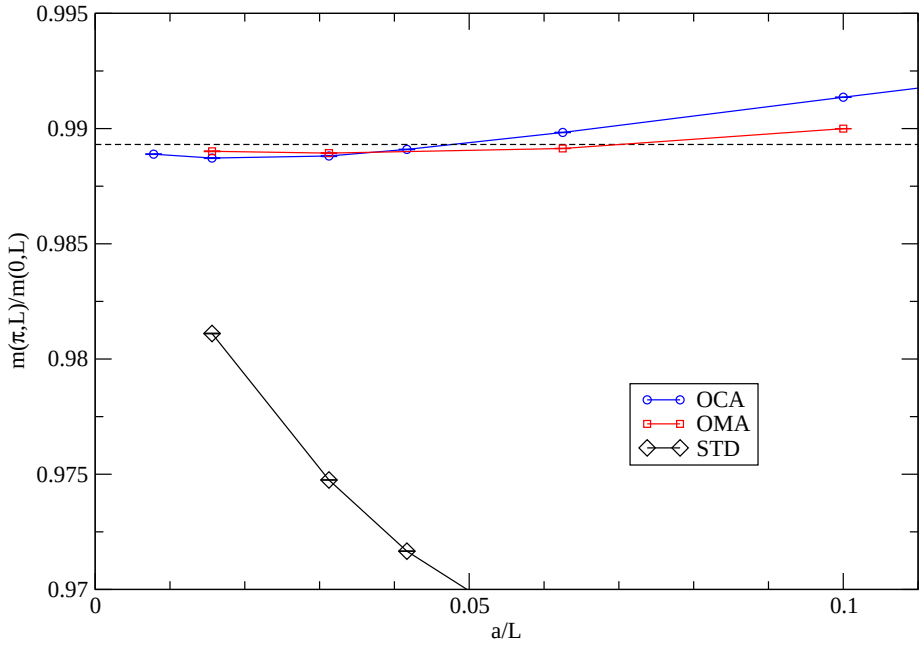

Figure 6. *Cutoff dependence of the mass gap ratio* $m(\theta = \pi, L)/m(0, L)$ *at fixed* $Lm(0, L) = u_0 = 1.0595$ *for the standard, constrained (with* $\cos\delta = -0.345$*), and optimized mixed action. The horizontal line is the analytic result.*

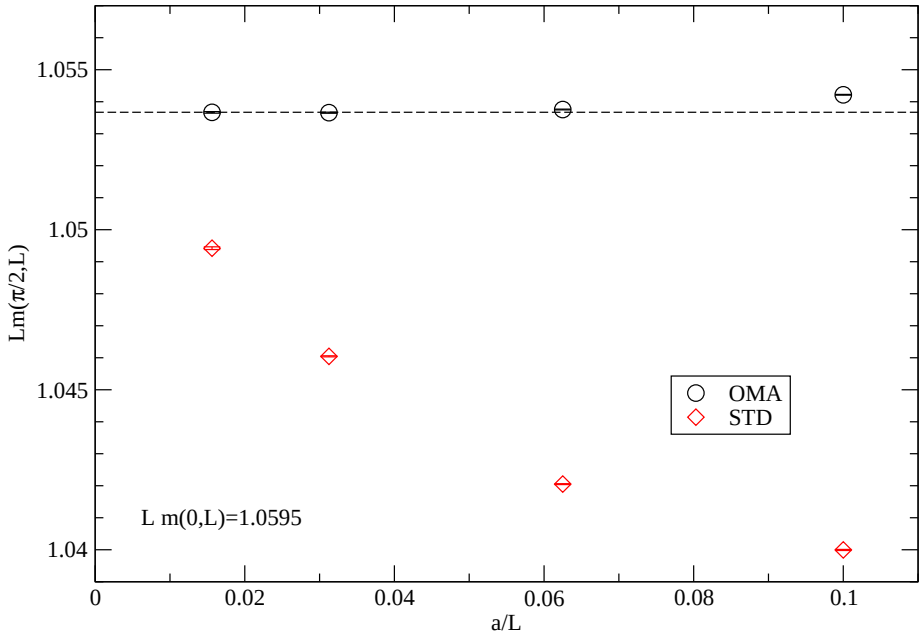

Figure 7. *Cutoff dependence of* $Lm(\theta, L)$ *at fixed* $Lm(0, L) = u_0 = 1.0595$*, for the standard and for the optimized mixed action at* $\theta = \pi/2$*. The horizontal line represents the fitted continuum value.*

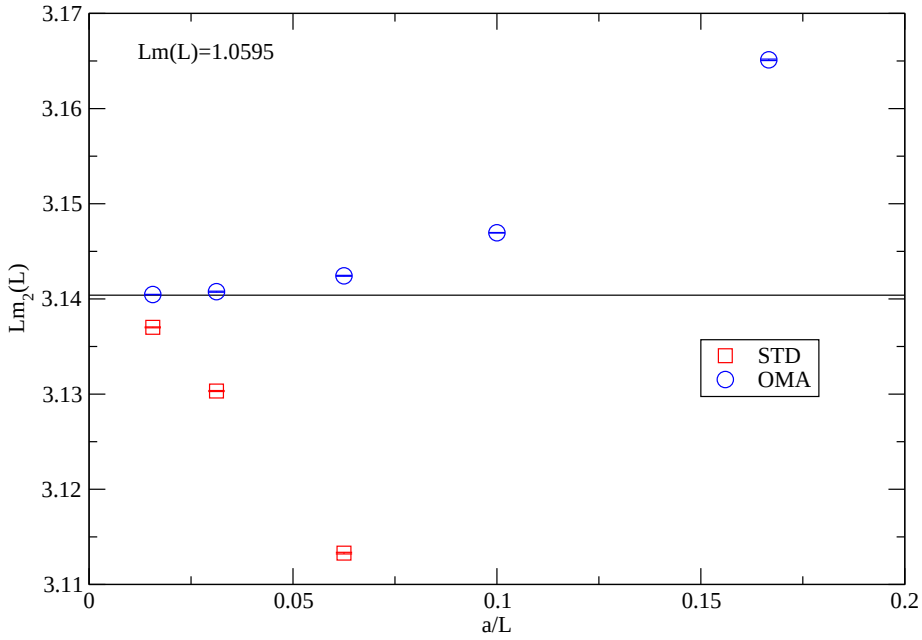

Figure 8. *Cutoff effects of the mass of the isotensor state for the standard and optimized mixed action (with the parameters listed in table 1).*

3.3 The mass of the isotensor state

Besides the state in the isovector channel, the exact S-matrix also provides analytic results for the finite-volume mass $m_2(L)$ in the isotensor channel ($I = 2$). Its approach to the continuum limit is shown in figure 8 for both the optimized mixed and the standard action. Again, the optimized mixed action reaches the continuum limit much faster than the standard action.

3.4 The renormalized coupling g_{R}

The renormalized coupling defined in terms of a truncated 4-point function at zero momentum (see eq. (5.44)), has been calculated from the exact S-matrix in [42] with the result $g_{\mathrm{R}} = 6.770(17)$. As illustrated in figure 9, without any further tuning of the optimized actions, the continuum limit of g_{R} is approached much more quickly with the optimized constrained and the optimized mixed action than with the standard or the topological action. The results from the optimized actions suggest that the theoretical error given in [42] has been overestimated. Based on the last two points with the optimized mixed action here we obtain the value $g_{\mathrm{R}} = 6.769(2)$.

4 Numerical Study of Cutoff Effects in the 2-d O(4) and O(8) Models

In order to investigate whether highly optimized local actions can also be constructed successfully for larger values of N, in this section we study the 2-d O(4) and the 2-d O(8) model. In these cases we limit ourselves to the optimized constrained action compared to the standard action.

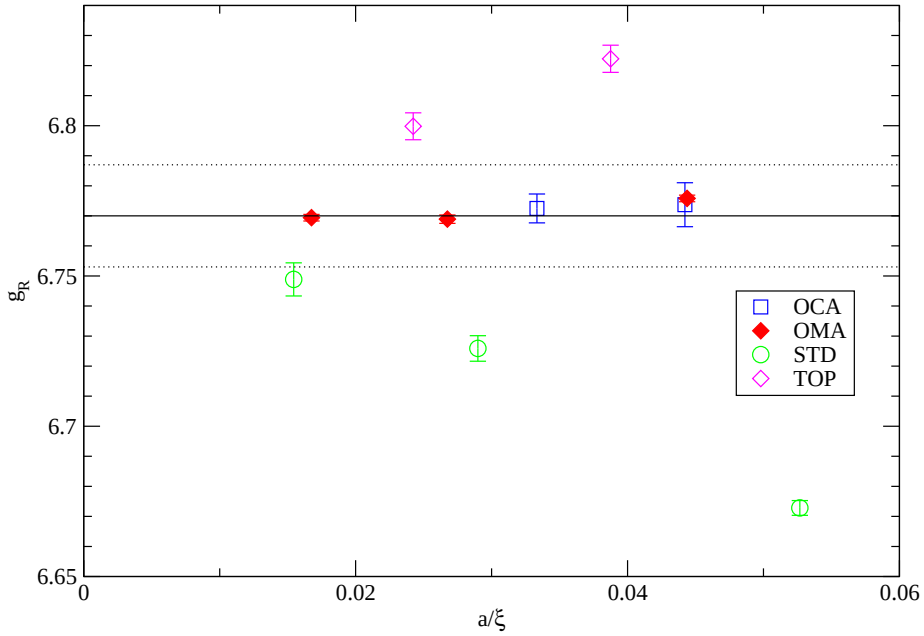

Figure 9. *Cutoff effects of the renormalized coupling g_R for four different lattice actions. The thick horizontal line is the result $g_R = 6.770(17)$ obtained from the exact S-matrix (whose estimated theoretical error corresponds to the dotted horizontal lines) [42].*

4.1 The step scaling function of the 2-d O(4) model

Figure 10 compares the cutoff effects of the step 2 scaling function for the standard action with those of the optimized constrained action. The constraint angle δ has been optimized by demanding $\Sigma(2, u_0, a/L = 1/10) = \sigma(2, u_0)$, in this case for $u_0 = 1$, which yields $\cos\delta = -0.096$. Again, the cutoff effects are drastically reduced in comparison to the standard action. Still, there are remaining tiny cutoff effects in the per mille range. The cutoff effect is not monotonic, after a small increase it starts to diminish only on an $L/a = 32$ lattice. The data for the standard action are taken from [18].

4.2 The step scaling function of the 2-d O(8) model

Figure 11 shows the analogous results for the O(8) case. In this case, the constraint is $\cos\delta = 0.217$, again for $u_0 = 1.0595$. The data for the standard action are from [17].

5 Analytic Study of Cutoff Effects in the 2-d O(N) Model at $N = \infty$

The step scaling function for the O(N) non-linear sigma model in the limit $N \to \infty$ has been studied in [17, 43, 44]. Here we generalize these calculations for the case of the constrained action and of the mixed action. Note that here we use lattice units, "$a = 1$".

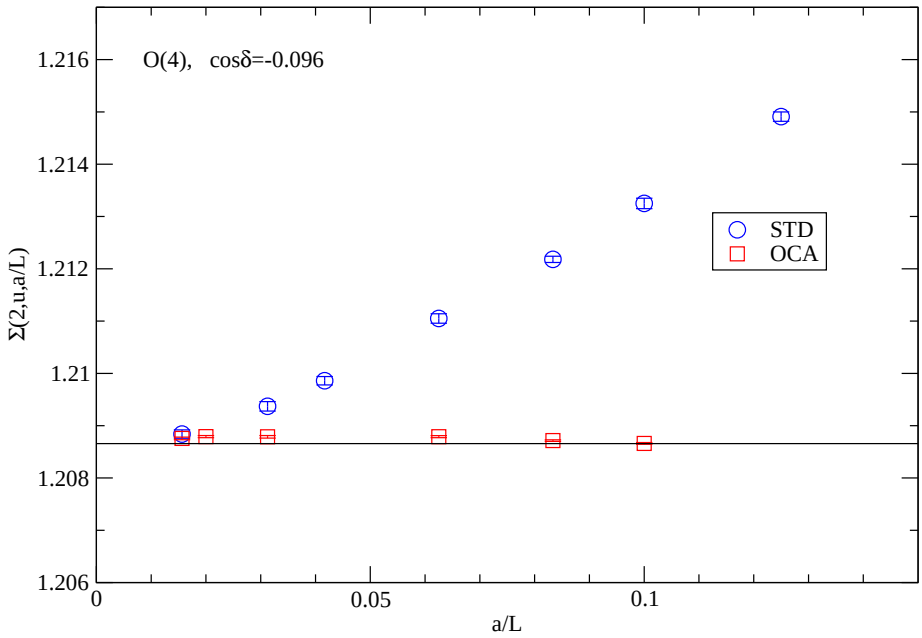

Figure 10. *Cutoff effects of the step-scaling function in the 2-d* O(4) *model. The horizontal line indicates the exact result in the continuum limit,* $\sigma(2, 1.0) = 1.208658$. *The optimized constrained action has cutoff effects in the fraction of a per mille range.*

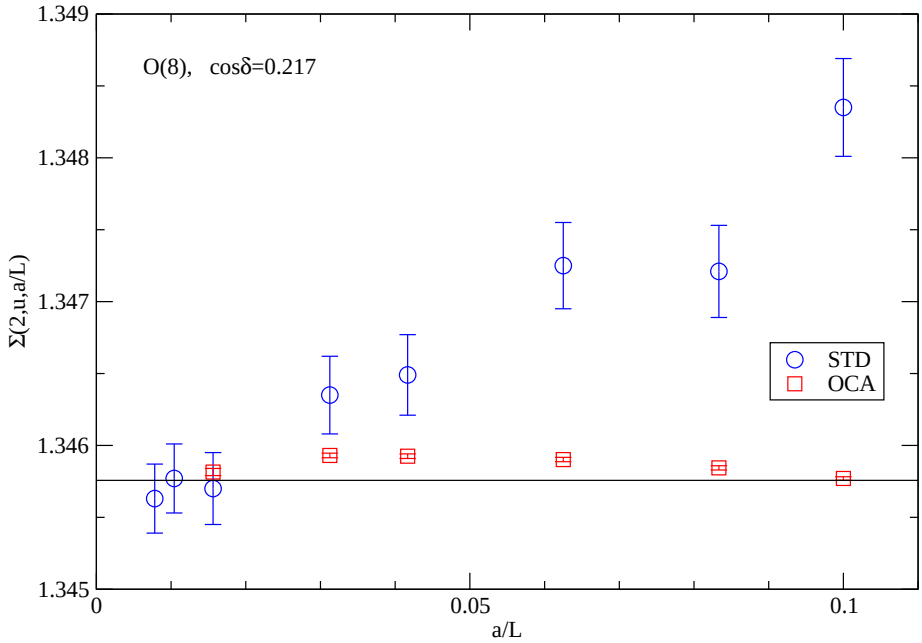

Figure 11. *Cutoff effects of the step-scaling function in the 2-d* O(8) *model. The horizontal line indicates the exact result in the continuum limit,* $\sigma(2, 1.0595) = 1.345757$. *The optimized constrained action has cutoff effects in the fraction of a per mille range.*

5.1 Constrained action in the large N limit

The action and the partition function in the constrained case are given by

$$S[\vec{e}] = \frac{N}{2f} \sum_{x,\mu} (\partial_\mu \vec{e}_x)^2 \,, \tag{5.1}$$

$$Z = \int_{\vec{e}} \exp\Big\{ - S[\vec{e}] \Big\} \prod_x \delta(\vec{e}_x^{\,2} - 1) \prod_{x,\mu} \Theta(\epsilon - (\partial_\mu \vec{e}_x)^2) \,. \tag{5.2}$$

Here Θ is the step function, ∂_μ denotes the forward lattice derivative, and $\int_{\vec{e}}$ denotes $\int \prod_x \mathrm{d}\vec{e}_x$. As usual, the $N \to \infty$ limit is taken with $\beta/N = 1/f$ fixed.

For the standard action the distribution of $(\partial_\mu \vec{e}_x)^2$ in the large N limit approaches a δ-function at $(\partial_\mu \vec{e}_x)^2 = f/d$ (where d is the number of Euclidean dimensions), as can be easily obtained from perturbation theory. On the other hand, for the topological action (with only the Θ-constraint, i.e. with $f = \infty$) it goes also to a δ-function at $(\partial_\mu \vec{e}_x)^2 = \epsilon$. One expects that for $\epsilon > f/d$ the constraint is irrelevant (it is above the narrow peak) and f alone determines the physics in the large N limit. On the contrary, at $\epsilon < f/d$ the constraint dominates the physics. It is also clear from these considerations that at $N = \infty$ the $\Theta(\epsilon - (\partial_\mu \vec{e}_x)^2)$ factors can be replaced by a strict constraint $\delta(\epsilon - (\partial_\mu \vec{e}_x)^2)$.

Introducing the auxiliary variables α_x, $\eta_{x\mu}$ one gets

$$Z = \int_{\vec{e},\alpha,\eta} \exp\Big\{ - S[\vec{e}] + i(\alpha, \vec{e}^{\,2} - 1) + i(\eta, \epsilon - (\partial \vec{e})^2) \Big\} \frac{1}{\eta - i0} \,. \tag{5.3}$$

Here the auxiliary variables are integrated over the real axis.

Note that $\epsilon = 2(1 - \cos\delta)$ where δ is the maximal allowed angle between the nearest neighbors. The allowed range is $0 < \epsilon \leq 4$. For $\epsilon \geq 4$ one recovers the standard (unconstrained) action.

Rescaling α and η as

$$\alpha_x \to \frac{1}{2} N \alpha_x \,, \qquad \eta_{x\mu} \to \frac{1}{2} N \eta_{x\mu} \,, \tag{5.4}$$

and then shifting the integration contour[1]

$$\alpha_x \to ih + \frac{\alpha_x}{\sqrt{N}} \,, \qquad \eta_{x\mu} \to -iv_\mu + \frac{\eta_{x\mu}}{\sqrt{N}} \,, \tag{5.5}$$

one obtains a form suitable for the $1/N$ expansion:

$$\begin{aligned} S_{\text{eff}} = \frac{N}{2} \Bigg[\sum_{x,\mu} \left(\frac{1}{f} + v_\mu \right) (\partial_\mu \vec{e}_x)^2 + h \sum_x \vec{e}_x^{\,2} - Vh - \epsilon V \sum_\mu v_\mu \Bigg] \\ - i \frac{\sqrt{N}}{2} \Big[\sum_x \alpha_x (\vec{e}_x^{\,2} - 1) + \sum_{x,\mu} \eta_{x\mu} (\epsilon - (\partial_\mu \vec{e}_x)^2) \Big] + \sum_{x,\mu} \ln \left(v_\mu + i \frac{\eta_{x\mu}}{\sqrt{N}} \right) \,, \end{aligned} \tag{5.6}$$

[1] Due to eq. (5.3) the integration line of $\eta_{x\mu}$ can be shifted only downwards, i.e. one should have $v_\mu \geq 0$.

Note that in eq. (5.5) we have allowed for different values of v_μ in different directions. In symmetric volumes $V = L^d$ they can be replaced by a single v. For the step scaling function one should take the strip geometry, $\infty \times L^{d-1}$. Here one should expect different v_μ's in the time- and spatial directions.[2]

After integrating out the spin fields we get[3]

$$\overline{S}_{\text{eff}} = \frac{N}{2}\left[\text{tr}\ln S - Vh - V\epsilon\sum_\mu v_\mu\right] + \mathcal{O}\left(\sqrt{N}\right)\,, \tag{5.7}$$

with

$$S_{xy} = h\delta_{xy} + \sum_\mu w_\mu\left[2\delta_{xy} - \delta_{y,x+\hat{\mu}} - \delta_{y,x-\hat{\mu}}\right]\,, \tag{5.8}$$

$$w_\mu = \frac{1}{f} + v_\mu\,. \tag{5.9}$$

For the inverse we have

$$S^{-1}_{xy} = \frac{1}{V}\sum_p \frac{\mathrm{e}^{ip(x-y)}}{D(p)}\,, \tag{5.10}$$

$$D(p) = \sum_\mu w_\mu K_\mu(p) + h\,, \tag{5.11}$$

where the sum is over $p_\mu = 2\pi n_\mu/L_\mu\,,\ \ n_\mu = 0, 1, \ldots, L_\mu - 1$ and where $K_\mu(p) = 2(1 - \cos p_\mu)$.

Note that the $1/(\eta - i0)$ denominator (i.e. the logarithmic term in eq. (5.6)) does not enter in the $N = \infty$ limit, i.e. the Θ-constraint is effectively replaced by a δ-constraint, as discussed above.

Eq. (5.7) in leading order yields the gap equations

$$\frac{1}{V}\sum_p \frac{1}{D(p)} = 1\,, \tag{5.12}$$

$$\frac{1}{V}\sum_p \frac{K_\mu(p)}{D(p)} = \epsilon\,. \tag{5.13}$$

Consistency of these equations gives the relation

$$h + \epsilon\sum_\mu w_\mu = 1\,. \tag{5.14}$$

The finite volume mass gap $m(L)$ in the strip geometry $\infty \times L^{d-1}$ in leading order $1/N$ is given by

$$m_0 = 2\sinh\frac{m(L)}{2}\,, \tag{5.15}$$

[2]Note that one could avoid this complication by modifying the constraint to an "isotropic" one, $\Theta\left(\epsilon - \overline{(\partial\vec{e}_x)^2}\right)$, meaning that the average of $(\partial_\mu\vec{e}_x)^2$ over the $2d$ nearest neighbors should not exceed ϵ.

[3]In the leading order in $1/N$ we will not need the terms depending on the auxiliary fields α_x, $\eta_{x\mu}$. Hence they are not written out explicitly here.

where

$$m_0^2 = \frac{h}{w_0}\,. \tag{5.16}$$

Defining

$$u = m(L)L\,, \tag{5.17}$$

one has

$$m_0 = m_0(u,L) = 2\sinh\frac{u}{2L} = \frac{u}{L}\left(1 + \frac{u^2}{24L^2} + \ldots\right)\,. \tag{5.18}$$

The continuum limit is approached by $L \to \infty$ keeping u fixed.

5.1.1 The isotropic case

In a symmetric volume L^d (or with the modified "isotropic action") one has $v_\mu = v$ and the gap equations (5.12), (5.13) yield

$$\frac{1}{V}\sum_p \frac{1}{K(p) + m_0^2} = \frac{1}{m_0^2 + \epsilon d}\,, \tag{5.19}$$

as well as the relation

$$\left(v + \frac{1}{f}\right)\epsilon d + h = 1\,. \tag{5.20}$$

Since one should have h and v non-negative, this relation has a solution only for $\epsilon \le f/d$. As discussed above, for larger ϵ the kinetic term is the relevant one and the constraint can be omitted. As expected, the gap equation (5.19) has a solution only for $\epsilon < 4$ since for the standard action $0 \le K(p) \le 4$.

For the standard (unconstrained) action the gap equation reads

$$\frac{1}{V}\sum_p \frac{1}{K(p) + m_0^2} = \frac{1}{f}\,. \tag{5.21}$$

In the infinite volume eq. (5.19) gives

$$\int_{-\pi}^{\pi} \frac{\mathrm{d}^d p}{(2\pi)^d}\frac{1}{K(p) + m_0^2} = \frac{1}{m_0^2 + \epsilon d}\,. \tag{5.22}$$

From now on we consider the $d = 2$ case. In this case the integral on the l.h.s. of eq. (5.22) diverges logarithmically like $1/(4\pi)\log(a^2 m_0^2)$, where we restored the lattice spacing. For the standard action this gives the well known result

$$m \approx \frac{\text{const}}{a}\mathrm{e}^{-2\pi/f}\,. \tag{5.23}$$

Since $m_0^2 \propto \exp(-2\pi/\epsilon)$ in the continuum limit $\epsilon \to 0$ the m_0^2 term can be neglected on the r.h.s. of eqs. (5.19), (5.22), and in the continuum limit one recovers the universal result. The cutoff effects will be, however, slightly different. To determine them for the step scaling function one can solve the gap equation (5.19) numerically in a finite volume for different lattice spacings (i.e. different L/a). It turns out that the leading $\mathcal{O}(a^2)$ cutoff effects can be calculated analytically.

5.1.2 The lattice artifacts at $N = \infty$ for the step scaling function

Consider the $d = 2$ case in the strip geometry $\infty \times L$ and introduce

$$\rho = \frac{w_1}{w_0}\,, \tag{5.24}$$

$$\omega = \rho K_1(p) + m_0^2\,. \tag{5.25}$$

Writing eqs. (5.12), (5.13) for $L_t = \infty$ after integrating out p_0 one obtains a set of two equations

$$\frac{1}{L}\sum_p \frac{1}{\sqrt{\omega(\omega+4)}} = w_0\,, \tag{5.26}$$

$$\frac{1}{L}\sum_p \frac{K_1(p)}{\sqrt{\omega(\omega+4)}} = \epsilon w_0\,, \tag{5.27}$$

where from eq. (5.14) one has $w_0 = 1/[m_0^2 + (\rho+1)\epsilon]$.

We are interested in the approach of the step scaling function $u'(u, L) = m(2L)2L$ for fixed $u(L) = m(L)L$ to the continuum limit $a/L \to 0$. Analytic results are obtained using the results of Caracciolo and Pelissetto [44]; technical details are deferred to appendix B.1. The result is of the form

$$u' = u'_\infty + \frac{1}{L^2}\nu(u, z) + \dots\,, \tag{5.28}$$

where the continuum limit $u'_\infty = \sigma(2, u)$ is (the same for all actions) given by the solution of the relation

$$f_0(u) = f_0(u'_\infty) + \frac{1}{2\pi}\ln 2\,, \tag{5.29}$$

where the function $f_0(u)$ is specified in eq. (B.12). The lattice artifacts depend on the lattice actions; the leading artifacts are specified by the function $\nu(u, z)$ where, as will be seen later, it is convenient to express the $\ln L$ dependence through z defined by

$$z = z(u, L) = f_0(u) + \frac{1}{2\pi}\ln L\,. \tag{5.30}$$

Considering first the standard action, the leading lattice artifacts are linear in z:

$$\nu_{\rm std}(u, z) = t_0(u) + t_1(u)z\,, \tag{5.31}$$

where the functions $t_0(u), t_1(u)$ are specified in eqs. (B.22), (B.23). The coefficient $t_1(u)$ is positive, so the asymptotic approach to the continuum limit is always from above. Numerical evaluation shows that $t_0(u)$ is negative for all u, hence the two terms compete with each other. It turns out that $\nu_{\rm std}(u, L)$ is positive at $u > 0.6357$ for any L. Below this value the approach for reasonable L seems (misleadingly) to be from below. For small u the asymptotic behavior sets in only at very large L/a, e.g. at $u = 0.3$ the coefficient $\nu_{\rm std}(u, L)$ becomes positive only for $L/a \gtrsim 10^5$.

Turning to the constrained action, one can calculate the infinite volume correlation length ξ for this case. For large L one gets from eqs. (B.3), (B.5)

$$\frac{1}{2\epsilon} = z + \mathcal{O}\left(1/L^2\right)\,. \tag{5.32}$$

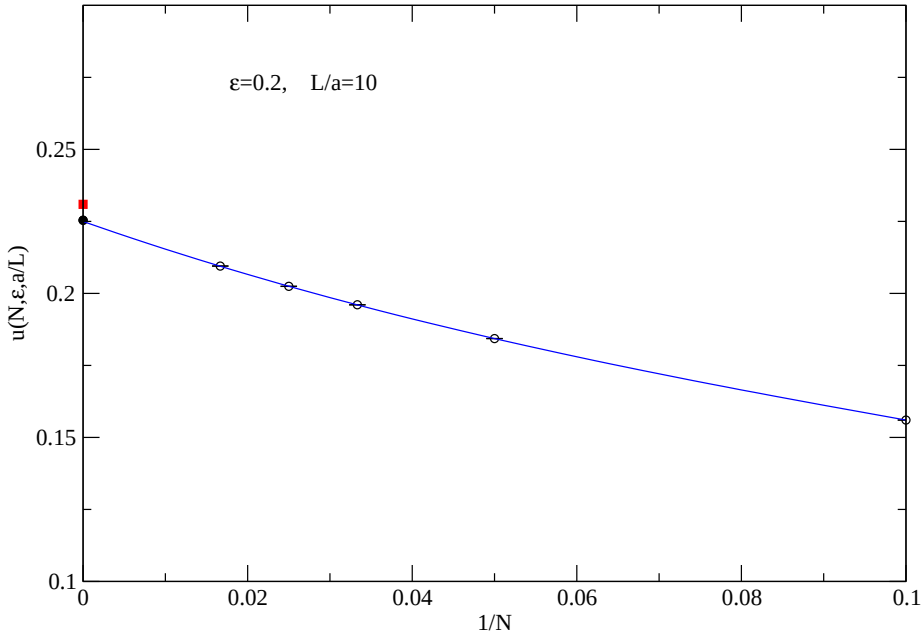

Figure 12. $u(\epsilon, L)$ for the O(N) topological action at large N values. The line is a cubic fit to the 5 data points. The two points at $1/N = 0$ show the results obtained from solving the gap equations numerically. The lower point is obtained from eqs. (5.26), (5.27). For comparison we also give the result for the "isotropic action", eq. (5.19), upper point.

Using the asymptotic expression for large $u = m(L)L \approx ML$

$$f_0(u) = -\frac{1}{2\pi} \ln u + \frac{5}{4\pi} \ln 2 + \mathcal{O}\left(\mathrm{e}^{-u}\right) , \tag{5.33}$$

one obtains

$$\frac{1}{2\epsilon} = \frac{1}{2\pi} \ln(\sqrt{32}\,\xi) \left[1 + \mathcal{O}\left(\xi^{-2}\right)\right] . \tag{5.34}$$

This is the same relation as for the standard action [43] when the coupling f is replaced by 2ϵ.

First, one can solve the coupled equations determining the step scaling function for the constrained action numerically as indicated in appendix B.1.1. We checked the numerical solution by direct Monte Carlo measurements for the constrained topological action ($f = \infty$) at $\epsilon = 0.2$, $L = 10$ for $N = 10, 20, 30, 40, 60$. The results are shown in figure 12. The value extrapolated to $N = \infty$ is 0.225(1). It agrees with the solution of the coupled gap equations, $u(0.2, 10) = 0.225410$. For the anisotropy parameter in this case one obtains $\rho = 0.950485$. (Note that for the isotropic model, eq. (5.19) one gets a slightly different value, $u(0.2, 10) = 0.230919$.)

One can also proceed analytically (see appendix B.1.2) and one finds that the lattice artifact $\nu_{\mathrm{con}}(u, L)$ is now quadratic in z:

$$\nu_{\mathrm{con}}(u, z) = \bar{t}_0(u) + \bar{t}_1(u) z + \bar{t}_2(u) z^2 , \tag{5.35}$$

where the functions $\bar{t}_i(u)$ are given in eq. (B.29). Comparing this to the result for the standard action, one has

$$\bar{t}_2(u) = -8t_1(u)\,, \tag{5.36}$$

i.e. the asymptotic approach of u' to its asymptotic value for the constrained action is always opposite to that of the standard action, so that the approach in this case is always from below. This behavior is essentially the same as observed for the O(3) case.

We remark that the $\ln^2 L$ behavior found above is not in contradiction to the analysis of ref. [40], since the constrained action does not belong to the class of actions considered there.

5.2 Mixed action in the large N limit

Here we consider the mixed action

$$S_{\rm mix}[\vec{e}] = \frac{\beta}{2}\sum_{x,\mu}(\partial_\mu \vec{e}_x)^2 + \frac{\gamma}{4}\sum_{x,\mu}[(\partial_\mu \vec{e}_x)^2]^2\,. \tag{5.37}$$

It has the advantage over the constrained action that the cutoff effects can be changed continuously, and in particular, tuned to zero for a given quantity, similar to the O(3) case discussed in section 3.

We shall take the large N limit as

$$\beta = \frac{N}{f}\,, \qquad \gamma = \frac{2N}{\kappa^2}\,. \tag{5.38}$$

The $1/N$ expansion is obtained similarly to the case of the constrained action and is described in appendix B.2.

Introducing the effective coupling $\hat{f} = \hat{f}(f,\kappa)$ by

$$\frac{1}{\hat{f}} = \frac{1}{2f} + \sqrt{\frac{1}{4f^2} + \frac{1}{\kappa^2}}\,, \tag{5.39}$$

similarly to the constrained case (cf. eqs. (5.32)–(5.34)) one finds for the infinite volume correlation length

$$\frac{1}{\hat{f}} = \frac{1}{2\pi}\ln(\sqrt{32}\,\xi)\left[1 + \mathcal{O}\left(\xi^{-2}\right)\right]\,. \tag{5.40}$$

Besides $\hat{f}$ we introduce

$$r = \frac{\kappa}{f}\,, \qquad \text{and} \quad q = \frac{1}{2}\left(r + \sqrt{r^2+4}\right)\,. \tag{5.41}$$

The fixed points in the coupling space are those where $\hat{f}(f,\kappa) = 0$, i.e. the boundaries of the first quadrant of the f, κ plane. The continuum limit of the step scaling function, $u'_\infty = \sigma(2,u)$ is of course universal, but the cutoff effects depend on the ratio r, in general on the particular path $r(\hat{f})$ along which one approaches to the continuum limit.

In appendix B.2 it is shown that the leading artifact is of the form

$$\nu_{\rm mix}(u,z) = T_0(u) + T_1(u)z + T_2(u)z^2\,, \tag{5.42}$$

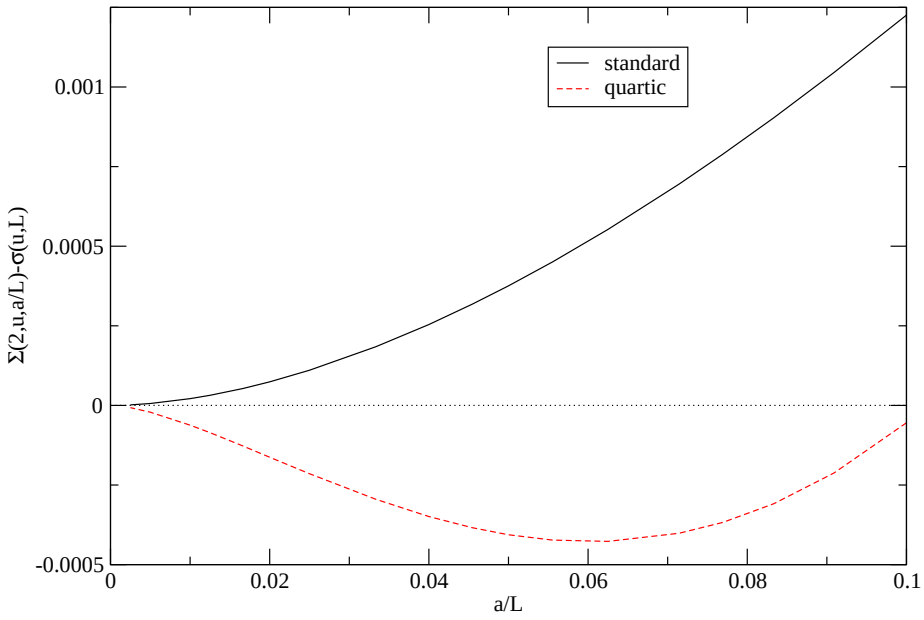

Figure 13. Deviation of $\Sigma(2, u, a/L)$ from the exact value for the standard and quartic action.

with functions $T_i(u)$ specified in eqs. (B.53), (B.54).

One notes that the coefficients appearing in $T_0(u)$ and $T_2(u)$ depend on the ratio r. For $r =$ constant the cutoff coefficient $\nu_{\rm mix}(u, z)$ is in general a second order polynomial in z (i.e. in $\ln L$, cf. eq. (5.30)). The exception is the standard action ($r = \infty$) where it is a first order polynomial. In this case one recovers eqs. (5.31) and (B.23), as expected. The purely quartic action is obtained by setting $r = 0$.

The leading cutoff effect is positive for the standard action, and (for fixed r) negative in other cases. Figure 13 shows the deviation $\Sigma(2, u, a/L) - \sigma(2, u)$ for the standard and quartic action (with $\kappa = \infty$ and $f = \infty$, respectively.)

As one can see from eqs. (5.41), (B.54), for large z one can cancel the artifact by choosing r a function of $\hat{f}$ so that asymptotically $q^2 = 8z + \mathcal{O}(1)$. This gives for large L the optimal path

$$\frac{\kappa^2}{2f} = \frac{\beta}{\gamma} \approx 4\,. \tag{5.43}$$

Note that the cancellation between the z and z^2 terms takes place for all values of u and scale factors s, hence the lattice artifact $\Sigma(s, u, a/L) - \sigma(s, u)$ is expected to be significantly reduced for all s and u once it is removed, say, for $s = 2$, $u = 1$.

The optimal path in the f, κ plane shown in figure 14 is determined from the condition $\Sigma(2, u, a/L) = \sigma(2, u)$ using eqs. (B.43)–(B.45). The dashed line corresponds to $\kappa^2/(2f) = 4$. Figure 15 shows the deviation $\Sigma(3, u, a/L) - \sigma(3, u)$ for the optimized values f, κ.

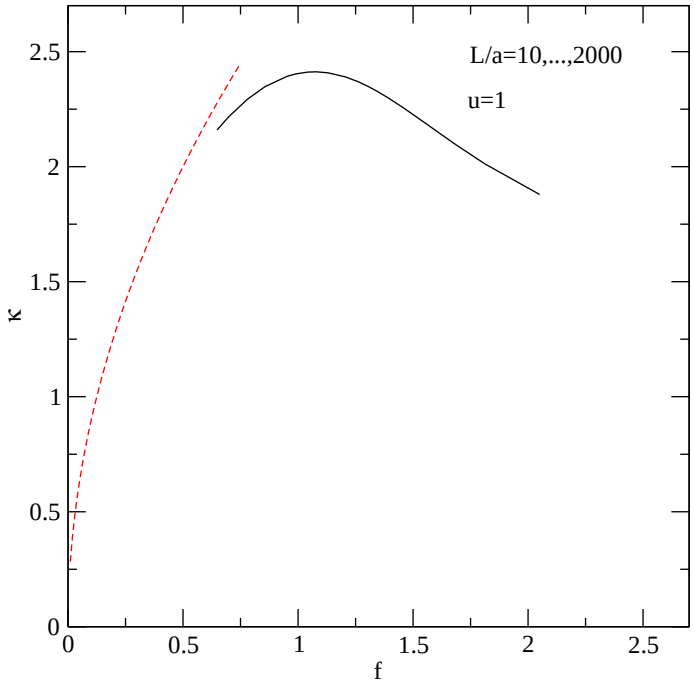

Figure 14. The curve of the optimal couplings determined from $\Sigma(2, u, a/L)$ at $u = 1$ for $N = \infty$. The solid curve shows the results for $L/a = 10, \ldots, 2000$, the dashed line shows the asymptotic dependence, $\kappa = \sqrt{8f}$.

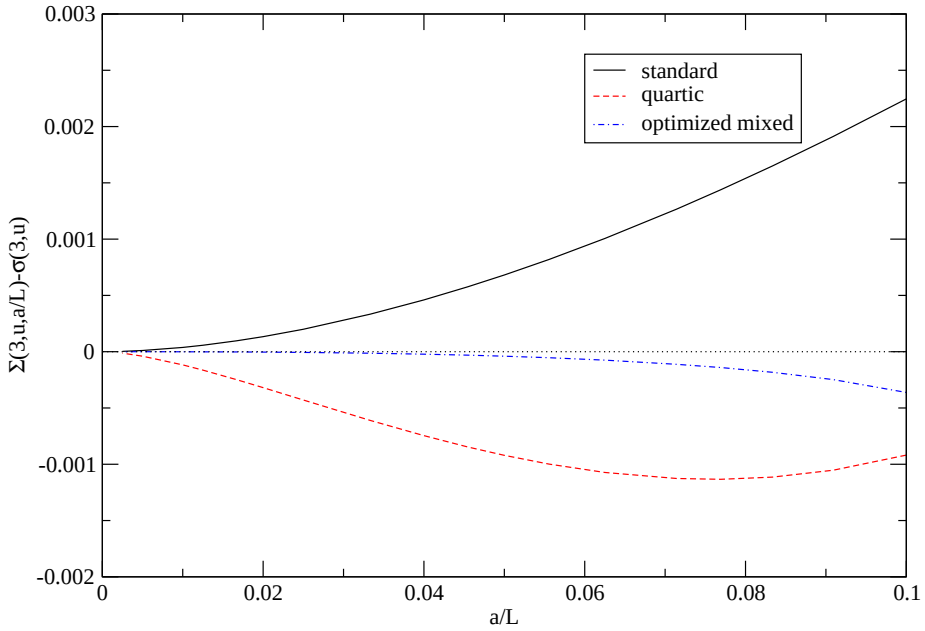

Figure 15. Deviation of $\Sigma(3, u, a/L)$ from the exact value for the standard, quartic and optimized mixed action. For the latter the couplings are determined to have $\Sigma(2, u, a/L) = \sigma(2, u)$.

5.2.1 The renormalized 4-point coupling

Here we consider the renormalized 4-point coupling at zero momentum, $g_{\rm R}$, defined through the Binder cumulant:

$$g_{\rm R} = -\frac{VM^2}{\Sigma^2} \sum_{x,y,x',y'} \langle \vec{e}_x \cdot \vec{e}_y \; \vec{e}_{x'} \cdot \vec{e}_{y'} \rangle_c \,, \tag{5.44}$$

$$\Sigma = \sum_{x,y} \langle \vec{e}_x \cdot \vec{e}_y \rangle \,, \tag{5.45}$$

and M is some renormalized mass:

$$M = m_0 + \mathcal{O}(1/N) \,. \tag{5.46}$$

Since $g_{\rm R} = \mathcal{O}(1/N)$ for large N one needs a calculation at order $1/N$ which is described in appendix B.2.1.

Taking the infinite volume limit and the continuum limit, the lattice artifacts are given by (see appendix B.2.2)[4]

$$N g_{\rm R}(aM) = 8\pi + a^2 M^2 A(q, \mathcal{L}) + \mathcal{O}(a^4 M^4) \,, \tag{5.47}$$

where $\mathcal{L} = -\ln(M^2/32)$ and

$$A(q, \mathcal{L}) = 2\pi + \frac{2}{1+q^2} - \left(\pi + \frac{4}{1+q^2}\right) \mathcal{L} + \frac{2}{1+q^2} \mathcal{L}^2 \,. \tag{5.48}$$

Here q is given by eq. (5.41).

We see that the artifacts in $g_{\rm R}$ behave very similarly to the step scaling function artifacts (except that they are of opposite sign) in that the leading artifact is $\mathcal{O}(a^2 M^2)$ times a second order polynomial in $\ln(aM)$.

Approaching the continuum limit along the curve $\kappa^2/(2f) = 4$ (cf. eq. (5.43)), for which the logarithmic terms in the step scaling function cancel, we have $q^2 = 1 + 8w$, and a similar cancellation occurs here.

The numerical evaluation of $N g_{\rm R}$ in the infinite volume limit is described in appendix B.2.3. Figure 16 shows the deviation $N g_{\rm R}(aM) - 8\pi$ as a function of aM.

6 Conclusions

We have investigated a variety of lattice actions in numerical simulations of 2-d O(3), O(4), and O(8) models, as well as analytically at $N = \infty$. By optimizing the constraint angle δ or the quartic coupling γ in very simple nearest-neighbor actions that suppress large field fluctuations, we have obtained a class of lattice actions with extremely small cutoff effects, often in the fraction of a per mille range. The simplicity of these actions makes them very useful for numerical simulations. In particular, the Wolff cluster algorithm is applicable in a straightforward manner.

[4] Here we re-introduce the lattice spacing a.

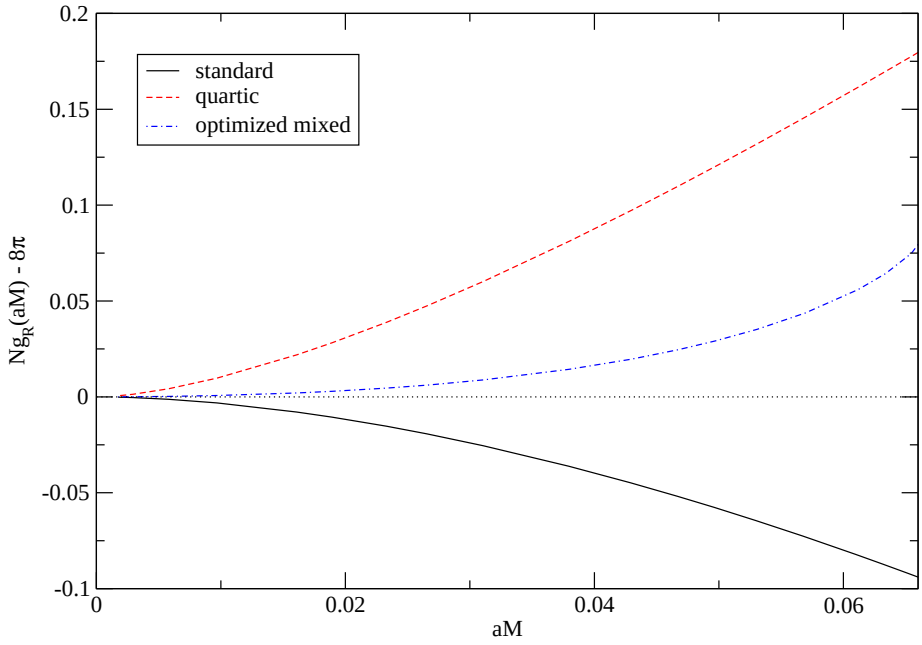

Figure 16. $Ng_{\rm R} - 8\pi$ for the standard, quartic and optimized mixed action

It is pointed out in [20] and also observed here, that in order to belong to the corresponding universality class an action is not required to have the standard classical continuum limit.

Interestingly, both the constrained action and the mixed action have unexpected cutoff effects at $N = \infty$. In particular, the leading artifact in both cases is $\sim a^2 \log^2(aM)$ while for the class of lattice actions considered in [40] in the framework of Symanzik's effective theory the leading artifact is $\sim a^2 \log(aM)$.

Although this might appear as a puzzle at first sight, in fact Symanzik's effective theory approach is valid also for the actions considered here. In this framework the lattice artifacts are described by the effective continuum Lagrangian

$$\mathcal{L}_{\rm arti} = a^2\, C\, O_4 \tag{6.1}$$

where the c-number coefficient C is coupling-dependent and O_4 is a local O(N)-invariant operator. (In fact the complete artifact Lagrangian is a linear combination of several terms of this form.) Approaching the continuum limit along a given curve in coupling space, C becomes a function of the inverse correlation length aM. On the other hand the matrix elements of the operator O_4 are cutoff-independent but depend on the physical parameters (u for the case of the step-scaling function). We know how to calculate the asymptotic form of the dependence on aM only if coupling constant perturbation theory is applicable.

The actions considered in [40] were perturbative — close to the continuum limit the fluctuation of the corresponding field was determined mainly by the quadratic part of the action. On the other hand, for the constrained action (for sufficiently small ϵ) these fluctuations are restricted by the constraint, while for the mixed action (for sufficiently

large γ) by the quartic term coming from $\gamma(\partial_\mu \vec{e})^4$, hence the situation is non-perturbative. (This is obvious for the topological action, which is zero for the allowed configurations.)

The large N results suggest that the coefficient C receives non-perturbative contributions, which behave as $\propto \log^2(aM)$ for $N \to \infty$. This scenario is supported by the fact that for these actions the $\log^2(aM)$ and the $\log(aM)$ terms have the same u-dependence (namely u^2, cf. eqs. (B.28), (B.54)) as the leading term for the perturbative actions (coming from the same operator). This issue deserves further investigation.

At large N for the standard action the squared fluctuation of the relative angle is roughly given by f, while in the case of the mixed action for the purely quartic case ($\beta = 0$, i.e. $f = \infty$) it is given by κ. If by taking the continuum limit the ratio $r = \kappa/f$ approaches infinity, then the fluctuations are dominated by the quadratic part of the action. In this case one observes indeed an $a^2 \log(a)$ artifact, as for the other perturbative actions. In particular, this is the case when one moves along the optimal curve $\kappa = \sqrt{8f}$, where even the leading $a^2 \log(a)$ artifact cancels. By taking the continuum limit along a straight line, $r = \text{const}$ both the quadratic and the quartic terms are relevant.[5] This case cannot be treated in perturbation theory, and produces a leading $a^2 \log^2(a)$ artifact.

It is remarkable that a very simple nearest-neighbor action can reduce cutoff effects that drastically, and it is obvious to ask whether this success extends to other interesting asymptotically free lattice field theories, including 2-d $\mathbb{C}\mathrm{P}(N-1)$ models, 4-d Yang-Mills theories, or even QCD. Optimized actions are straightforward to construct in all these cases, and investigations in this direction are currently in progress. Of course, there is no exact result that helps finding the optimalized values of the parameters in these cases. However, as was found here, determining the optimal choice of the parameters by calculating one physical quantity very precisely leads to an action where lattice artifacts are small for a large class of other physical quantities as well.

Acknowledgments

We like to thank C. Destri for useful discussions. This work is supported in part by funds provided by the Schweizerischer Nationalfonds (SNF). The "Albert Einstein Center for Fundamental Physics" at Bern University is supported by the "Innovations- und Kooperationsprojekt C-13" of the Schweizerische Universitätskonferenz (SUK/CRUS). J. B. and F. N. thank the MPI Munich, where part of this work has been done, for hospitality. This investigation has been supported in part by the Hungarian National Science Fund OTKA (under K 77400) and by the Regione Lombardia and CILEA Consortium through a LISA 2011 grant.

[5] This is also reflected by the expression for effective coupling $\hat{f}$, eq. (5.39).

A Analytic Study of Cutoff Effects in the 1-d O(3) Model

For the constrained action in one dimension the eigenvalues of the transfer matrix (with a properly chosen normalization factor) are given by

$$\lambda_n(\beta, c) = \int_c^1 \mathrm{d}z \, \mathrm{e}^{\beta(z-1)} P_n(z) \tag{A.1}$$

The standard action corresponds to $c = \cos\delta = -1$.

With the notation $x = 1/\beta$, $\epsilon = \exp((c-1)\beta)$:

$$\lambda_0 = x - \epsilon x \,, \tag{A.2}$$

$$\lambda_1 = x - x^2 - \epsilon(cx - x^2) \,, \tag{A.3}$$

$$\lambda_2 = x - 3x^2 + 3x^3 - \epsilon\left(\frac{1}{2}(3c^2-1)x - 3cx^2 + 3x^3\right) \,, \tag{A.4}$$

$$\lambda_3 = x - 6x^2 + 15x^3 - 15x^4 - \epsilon\left(\frac{1}{2}(5c^3-3c)x - \frac{1}{2}(15c^2-3)x^2 + 15cx^3 - 15x^4\right) \,. \tag{A.5}$$

The excitation energies of the rotator (in lattice units) are

$$aE_n = -\log\left(\frac{\lambda_n}{\lambda_0}\right) \,. \tag{A.6}$$

The lattice spacing is determined here by $aE_1 = 1$.

The ratios of the energies are given by

$$r_n = \frac{E_n}{E_1} \,. \tag{A.7}$$

In the continuum limit (c fixed, $\beta \to \infty$) they approach the well-known result for the quantum rotator,

$$\lim_{\beta\to\infty} r_n = \frac{1}{2}n(n+1) \,. \tag{A.8}$$

In particular

$$r_2 = 3 - x^2 - \frac{5}{2}x^3 + \ldots \tag{A.9}$$

$$r_3 = 6 - 5x^2 - \frac{25}{2}x^3 + \ldots \tag{A.10}$$

In the case of the topological action, $\beta = 0$, $c \to 1$, one has

$$r_2 = 3 + \frac{1}{2}(1-c) + \frac{3}{8}(1-c)^2 + \ldots \tag{A.11}$$

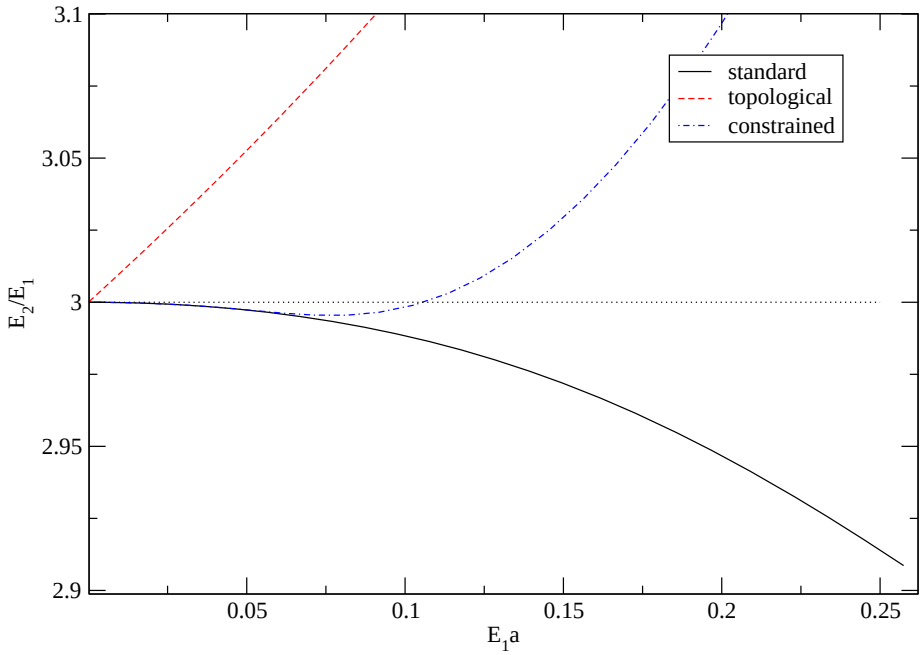

Figure 17. *The ratio of the mass gaps for the $I = 2$ and $I = 1$ states as a function of the lattice spacing for the standard, topological, and constrained action. For the latter the constraint is fixed at $E_1 a = 0.1$*

$$r_3 = 6 + \frac{5}{2}(1-c) + \frac{25}{8}(1-c)^2 + \ldots \tag{A.12}$$

Comparing eqs. (A.9),(A.10),(A.11), (A.12) one sees that the discretization errors for the standard action and for the the topological action have opposite signs. Fixing the constraint e.g. to $c = 0.4$ one obtains the resulting artifacts for r_2 which lie in between those for the standard and the topological action (cf. figure 17) An interesting possibility is to choose $c = c(\beta)$ in such a way that the first ratio is exact, $r_2(\beta, c(\beta)) = 3$. Of course, this procedure does not eliminate the discretization errors in other quantities, but it turns out that it improves the convergence to the continuum limit. Figure 18 shows $r_3(\beta, c(\beta)) - 6$ as a function of aE_1, which in a log-log plot looks nearly linear. From the numerical values one finds that $r_3(\beta, c(\beta)) - 6 \propto a^\alpha$, with the power $\alpha \approx 2.77$.

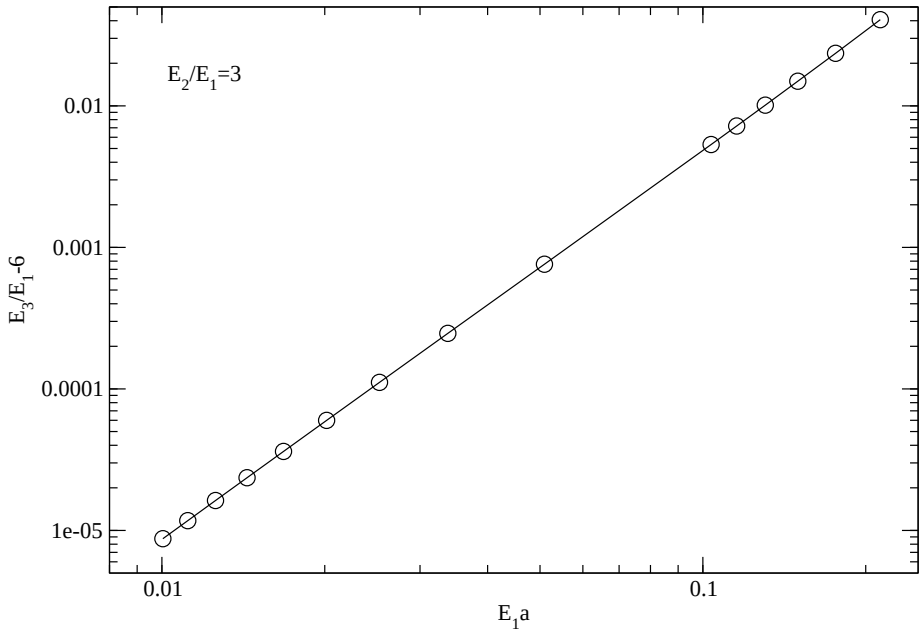

Figure 18. *The deviation of the ratio of the mass gaps for the I=3 and I=1 states from its continuum value. The constraint $c = c(\beta)$ is chosen so that $E_2/E_1 = 3$.*

B Technical Details of the $N = \infty$ Calculation

B.1 Analytic behavior of the step scaling function: constrained action

Introducing

$$I_1(\rho, u, L) = \frac{1}{L} \sum_p \frac{1}{\sqrt{\omega(\omega+4)}}\,, \tag{B.1}$$

$$I_2(\rho, u, L) = \frac{1}{L} \sum_p \frac{\omega}{\sqrt{\omega(\omega+4)}}\,, \tag{B.2}$$

(with m_0 given by eq. (5.18)) one obtains

$$I_1(\rho, u, L) = \frac{1}{m_0^2 + (\rho+1)\epsilon}\,, \tag{B.3}$$

$$I_2(\rho, u, L) = \frac{m_0^2 + \rho\epsilon}{m_0^2 + (\rho+1)\epsilon}\,. \tag{B.4}$$

The asymptotic expansion of I_1, I_2 can be obtained from the results of Caracciolo and Pelissetto [44] (expressing the expansion in terms of $u = mL$ instead of $m_0 L$ used therein). One has asymptotic expansions

$$I_1(\rho, u, L) = z + \frac{1}{L^2} B(u, z) + \dots\,, \tag{B.5}$$

$$I_2(\rho, u, L) = \frac{1}{2} + \frac{1}{L^2} D(u, z) + \dots\,, \tag{B.6}$$

where we recall z is defined by

$$z = z(u, L) = f_0(u) + \frac{1}{2\pi} \ln L \,, \tag{B.7}$$

and

$$B(u, z) = f_1(u) + \frac{1}{8} u^2 f_0(u) - \frac{1}{8} u^2 z - \frac{\rho_1}{2} \left[z + u f_0'(u) + \frac{1}{4\pi} \right] \,, \tag{B.8}$$

$$D(u, z) = f_2(u) - \frac{1}{2} u^2 f_0(u) + \frac{1}{2} u^2 z + \frac{\rho_1}{2\pi} \,. \tag{B.9}$$

Here ρ_1 appears in the expansion of $\rho(u, L)$

$$\rho(u, L) = 1 + \frac{1}{L^2} \rho_1(u, z) + \mathcal{O}\left(1/L^4\right) \,. \tag{B.10}$$

Note that the isotropy is recovered ($\rho \to 1$) for $L \to \infty$, as one can see from eq. (B.4) and from the infinite volume limit

$$I_2(\rho, u, \infty) = \frac{2}{\pi} \arctan\left(\sqrt{\rho}\right) \,. \tag{B.11}$$

The remaining L dependence in ρ_1 is assumed to be only logarithmic.
The functions $f_i(u)$ are given by

$$f_0(u) = \frac{1}{2u} + \frac{1}{2\pi} \left[k + G_0\left(\frac{u}{2\pi}\right) \right] \,, \tag{B.12}$$

$$f_1(u) = \frac{\pi}{6} \left[\frac{1}{12} - G_1\left(\frac{u}{2\pi}\right) \right] - \frac{u}{12} - \frac{u^2}{16\pi} \left[k + \frac{2}{3} G_0\left(\frac{u}{2\pi}\right) - \frac{1}{3} \right] \,, \tag{B.13}$$

$$f_2(u) = 2\pi G_1\left(\frac{u}{2\pi}\right) - \frac{\pi}{6} + \frac{u}{2} + \frac{u^2}{8\pi}(2k - 1) \,, \tag{B.14}$$

$$k = \gamma_E - \ln \pi + \frac{1}{2} \ln 2 \,. \tag{B.15}$$

We also need the derivative of $f_0(u)$:

$$f_0'(u) = -\frac{1}{2u^2} - \frac{u}{(2\pi)^3} H_1\left(\frac{u}{2\pi}\right) \,. \tag{B.16}$$

Here[6]

$$G_0(x) = \sum_{n=1}^{\infty} \left[\frac{1}{\sqrt{n^2 + x^2}} - \frac{1}{n} \right] \,, \tag{B.17}$$

$$G_1(x) = \sum_{n=1}^{\infty} \left[\sqrt{n^2 + x^2} - n - \frac{x^2}{2n} \right] \,, \tag{B.18}$$

$$H_1(x) = \sum_{n=1}^{\infty} (n^2 + x^2)^{-3/2} \,. \tag{B.19}$$

[6]Note there is an error in eq. (A.5) of [44]: it should read $G_1(\alpha) = 2 \sum_{k=1}^{\infty} \frac{(-1)^k}{k+1} \binom{2k}{k} \zeta(2k+1) \left(\frac{\alpha}{2}\right)^{2k+2}$.

Note for further reference that $f_0'(u) < 0$.

For the step scaling function we are interested in $u'(u, L) = m(2L)2L$ for fixed $u(L)$.

Consider first the standard action. From the gap equation $I_1(u, L) = 1/f$ and $I_1(u', 2L) = 1/f$ for $u' = u'(u, L)$ one has the equation

$$z + \frac{1}{L^2}\left[f_1(u) + \frac{1}{8}u^2 f_0(u) - \frac{1}{8}u^2 z\right] = z' + \frac{1}{4L^2}\left[f_1(u') + \frac{1}{8}u'^2 f_0(u') - \frac{1}{8}u'^2 z'\right] + \mathcal{O}(1/L^4)\,. \quad \text{(B.20)}$$

Expanding u' as in eq. (5.28) one sees that the continuum value u'_∞ is given by the solution to eq. (5.29).

From here and eq. (5.30) one has for $z' = z(u', 2L)$

$$z' = z + \frac{1}{L^2} f_0'(u'_\infty)\nu(u, z) + \mathcal{O}\left(\frac{1}{L^4}\right)\,. \quad \text{(B.21)}$$

Because of this relation one can replace z' by z in the $1/L^2$ terms in eq. (B.20). This is the reason for using z instead of $\ln L$.

For the leading lattice artifact one obtains eq. (5.31) where

$$t_0(u) = \frac{1}{f_0'(u'_\infty)}\left[f_1(u) + \frac{1}{8}u^2 f_0(u) - \frac{1}{4}\left(f_1(u'_\infty) + \frac{1}{8}u'^2_\infty f_0(u'_\infty)\right)\right]\,, \quad \text{(B.22)}$$

$$t_1(u) = -\frac{1}{8f_0'(u'_\infty)}\left[u^2 - \frac{1}{4}u'^2_\infty\right]\,. \quad \text{(B.23)}$$

Note that according to eq. (B.16) $f_0'(u)$ is negative for all u. Since $u'_\infty < 2u$ the coefficient $t_1(u)$ is positive.

B.1.1 Solving the coupled equations numerically

Eliminating ϵ from eqs. (B.3),(B.4) one gets (with m_0 given by eq. (5.18))

$$(1 + \rho)I_2(\rho, u, L) = m_0^2 I_1(\rho, u, L) + \rho\,. \quad \text{(B.24)}$$

This determines $\rho = \rho(u, L)$. Then one finds the corresponding ϵ by

$$\epsilon = \left(\frac{1}{I_1(\rho, u, L)} - m_0^2\right)\frac{1}{\rho + 1}\,. \quad \text{(B.25)}$$

Keeping ϵ fixed one can calculate $u' = u(\epsilon, 2L)$.

B.1.2 Analytic form of the leading artifact

Inserting the asymptotic expansions (B.5),(B.6),(B.10) we get

$$\rho_1(u) = \frac{2\pi}{\pi - 2}\left(2f_2(u) - u^2 f_0(u)\right)\,, \quad \text{(B.26)}$$

which is independent of z and

$$\frac{1}{2\epsilon} = \frac{\rho I_1}{2(I_2 - m_0^2 I_1)} = z + \frac{1}{L^2}\left(\Phi_0(u) + \Phi_1(u)z + \Phi_2(u)z^2\right) + \dots\,, \quad \text{(B.27)}$$

where

$$\begin{aligned}\Phi_0(u) &= f_1(u) + \frac{1}{8}u^2 f_0(u) - \frac{1}{2}\rho_1(u)\left(u f_0'(u) + \frac{1}{4\pi}\right), \\ \Phi_1(u) &= -\frac{1}{8}u^2, \\ \Phi_2(u) &= u^2 .\end{aligned} \tag{B.28}$$

One now obtains eq. (5.35) with

$$\bar{t}_i(u) = \frac{1}{f_0'(u_\infty')}\left(\Phi_i(u) - \frac{1}{4}\Phi_i(u_\infty')\right). \tag{B.29}$$

B.2 $1/N$ expansion for the mixed action

Here we discuss the mixed action given in eq. (5.37) in the large N limit given by eq. (5.38).

The partition function is

$$Z = \int_{\vec{e}} \exp\Big\{ - S_{\rm mix}[\vec{e}]\Big\} \prod_x \delta(\vec{e}_x^{\,2} - 1)\,. \tag{B.30}$$

Introducing the auxiliary variables α_x, $\eta_{x\mu}$ one obtains

$$S_{\rm eff}[\vec{e}] = \frac{1}{2}\sum_{x,\mu}(\beta + 2i\sqrt{\gamma}\eta_{x\mu})\,(\partial_\mu \vec{e}_x)^2 + \sum_{x,\mu}\eta_{x\mu}^2 - i\sum_x \alpha_x(\vec{e}_x^{\,2} - 1)\,. \tag{B.31}$$

Rescaling and shifting the integration contour as

$$\alpha_x \to \frac{1}{2}N\left(ih + \frac{\alpha_x}{\sqrt{N}}\right), \qquad \eta_{x\mu} \to \sqrt{\frac{N}{2}}\frac{\kappa}{2}\left(-iv_\mu + \frac{\eta_{x\mu}}{\sqrt{N}}\right), \tag{B.32}$$

one gets

$$\begin{aligned} S_{\rm eff}[\vec{e}] = \frac{1}{2}N\Bigg[\sum_{x,\mu}\left(\frac{1}{f} + v_\mu + i\frac{\eta_{x\mu}}{\sqrt{N}}\right)(\partial_\mu \vec{e}_x)^2 \\ + \frac{\kappa^2}{4}\sum_{x,\mu}\left(-iv_\mu + \frac{\eta_{x\mu}}{\sqrt{N}}\right)^2 + \sum_x\left(h - i\frac{\alpha_x}{\sqrt{N}}\right)(\vec{e}_x^{\,2} - 1)\Bigg]\,. \end{aligned} \tag{B.33}$$

Note that one has to allow for an anisotropy in v_μ because the lattice is not cubic, $L_t \neq L_s$.

After integrating out the spin fields we get an effective action in the auxiliary fields

$$\begin{aligned} \overline{S}_{\rm eff} = \frac{N}{2}\left[\mathrm{tr}\ln R - Vh - V\frac{\kappa^2}{4}\sum_\mu v_\mu^2\right] \\ - i\frac{\sqrt{N}}{2}\Big[-\sum_x \alpha_x + \frac{\kappa^2}{2}\sum_{x,\mu} v_\mu \eta_{x\mu}\Big] + \frac{\kappa^2}{8}\sum_{x,\mu}\eta_{x\mu}^2\,, \end{aligned} \tag{B.34}$$

with

$$R_{xy} = S_{xy} + \frac{i}{\sqrt{N}} T_{xy} \,, \tag{B.35}$$

$$S_{xy} = h\delta_{xy} + \sum_{\mu} w_{\mu} \left[2\delta_{xy} - \delta_{y,x+\hat{\mu}} - \delta_{y,x-\hat{\mu}} \right] \,, \tag{B.36}$$

$$T_{xy} = -\alpha_x \delta_{xy} + t_{xy} \,, \tag{B.37}$$

$$t_{xy} = \sum_{\mu} \left[\eta_{x\mu} \left(\delta_{xy} - \delta_{y,x+\hat{\mu}} \right) + \eta_{(x-\hat{\mu})\mu} \left(\delta_{xy} - \delta_{y,x-\hat{\mu}} \right) \right] \,, \tag{B.38}$$

$$w_{\mu} = \frac{1}{f} + v_{\mu} \,. \tag{B.39}$$

For the inverse S^{-1}_{xy}, and $D(p)$ we have the previous expressions, eqs. (5.10),(5.11).

In the leading order of $1/N$ expansion one obtains the following equations for h and v_μ

$$\frac{1}{V} \sum_{p} \frac{1}{D(p)} = 1 \,, \tag{B.40}$$

$$\frac{1}{V} \sum_{p} \frac{K_{\mu}(p)}{D(p)} = \frac{1}{2} \kappa^2 v_{\mu} \,. \tag{B.41}$$

This yields the relation

$$\frac{1}{2} \kappa^2 \sum_{\mu} v_{\mu} w_{\mu} + h = 1 \,. \tag{B.42}$$

For the $d = 2$ case, with the same notations as in the constrained case (cf. appendix B.1) we get for $L_t = \infty$:

$$I_1(\rho, u, L) = w_0 \,, \tag{B.43}$$

$$I_2(\rho, u, L) = w_0 \left(\frac{\kappa^2}{2} \rho v_1 + m_0^2 \right) \,, \tag{B.44}$$

and

$$\frac{1}{2} \kappa^2 (v_0 + \rho v_1) + m_0^2 = \frac{1}{w_0} \,. \tag{B.45}$$

Eliminating v_0, v_1 from eqs. (B.43),(B.44) and (B.45) we can express the two couplings in terms of u, L and the remaining saddle point parameter, ρ:

$$\frac{2}{\kappa^2} = \frac{\rho(\rho - 1)}{(1 + \rho) I_2 - \rho - m_0^2 I_1} I_1^2 \,, \tag{B.46}$$

$$\frac{1}{f} = I_1 + \frac{2}{\kappa^2} \cdot \frac{I_2 - 1}{I_1} \,. \tag{B.47}$$

Inserting the asymptotic expansions (B.5), (B.6) into eq. (B.47) one obtains

$$\frac{1}{f} = z - \frac{1}{\kappa^2 z} + \mathcal{O}\left(\frac{1}{L^2} \right) \,. \tag{B.48}$$

Solving this for z one finds

$$z(u,L) = \frac{1}{\hat{f}} + \mathcal{O}\left(\frac{1}{L^2}\right), \tag{B.49}$$

where the effective coupling $\hat{f}(f,\kappa)$ is defined in eq. (5.39).

Inserting the asymptotic expansions[7] (B.5), (B.6), and (B.10) into eq. (B.46), and using eq. (B.49) one obtains

$$\rho_1(u) = \frac{2(2f_2(u) - u^2 f_0(u))}{1 - \frac{2}{\pi} + q^2}, \tag{B.50}$$

up to $\mathcal{O}(L^{-2})$. Here q is a function of the coupling ratio $r = \kappa/f$ given by eq. (5.41). Note that taking $r = \infty$ one should recover the result for the standard action, while taking $r = 0$ that one for the pure quartic action.

We now eliminate I_2 using eq. (B.46) and obtain from eq. (B.47)

$$\frac{1}{f} = \frac{1}{1+\rho}\left\{(1+\rho^2)I_1 - \frac{2}{\kappa^2 I_1} + \frac{2m_0^2}{\kappa^2}\right\}. \tag{B.51}$$

Inserting the asymptotic expansions one obtains

$$\begin{aligned}\frac{1}{f} = z - \frac{1}{\kappa^2 z} + \frac{1}{L^2}\Bigg\{\Bigg[f_1(u) + \frac{1}{8}u^2 f_0(u) - \frac{1}{8}u^2 z \\ - \frac{1}{2}\rho_1(u)\left(u f_0'(u) + \frac{1}{4\pi}\right)\Bigg]\left(1 + \frac{1}{\kappa^2 z^2}\right) + \frac{u^2}{\kappa^2}\Bigg\} + \dots\end{aligned} \tag{B.52}$$

Using these relations one obtains the leading lattice artifacts given in eq. (5.42) with the functions $T_j(u)$ given by

$$T_i(u) = \frac{1}{f_0'(u_\infty')}\left(\Phi_i(u) - \frac{1}{4}\Phi_i(u_\infty')\right), \tag{B.53}$$

$$\begin{aligned}\Phi_0(u) &= f_1(u) + \frac{1}{8}u^2 f_0(u) - \frac{1}{2}\rho_1(u)\left(u f_0'(u) + \frac{1}{4\pi}\right), \\ \Phi_1(u) &= -\frac{1}{8}u^2, \\ \Phi_2(u) &= \frac{1}{1+q^2}u^2.\end{aligned} \tag{B.54}$$

B.2.1 The renormalized 4-point coupling in leading order

In order to compute at higher orders in the $1/N$ expansion let us introduce a source in the action;

$$S_{\text{eff}}[\vec{e},\vec{J}] = S_{\text{eff}}[\vec{e}] + \sum_x \vec{J}_x \cdot \vec{e}_x \tag{B.55}$$

Then after integrating out the spin fields we get

$$\overline{S}_{\text{eff}}[\vec{J}] = \overline{S}_{\text{eff}} - \frac{1}{2N}\sum_{x,y}\vec{J}_x (R^{-1})_{xy}\vec{J}_y. \tag{B.56}$$

[7] Using eqs. (B.46) and (B.11) one can show that $\rho(u,\infty) = 1$.

The propagators of the auxiliary fields are given by the quadratic terms

$$\overline{S}_{\text{eff,quadratic}} = \frac{1}{4}\text{tr}\left(S^{-1}TS^{-1}T\right) + \frac{\kappa^2}{8}\sum_{x,\mu}\eta_{x\mu}^2\,, \tag{B.57}$$

where S_{xy}^{-1} is given by eq. (5.10).

Defining the Fourier transforms

$$\alpha_x = \frac{1}{V}\sum_p \mathrm{e}^{ipx}\widetilde{\alpha}(p)\,, \tag{B.58}$$

$$\eta_{x\mu} = \frac{1}{V}\sum_p \mathrm{e}^{ip(x+\hat{\mu}/2)}\widetilde{\eta}_\mu(p)\,, \tag{B.59}$$

we have[8]

$$(TS^{-1})_{xy} = \frac{1}{V^2}\sum_{p,q}\frac{\mathrm{e}^{ip(x-y)+iqx}}{D(p)}\left\{-\widetilde{\alpha}(q) + \widehat{(p+q)}_\mu\hat{p}_\mu\widetilde{\eta}_\mu(q)\right\}\,, \tag{B.60}$$

so the quadratic term in the auxiliary fields is

$$\begin{aligned}\overline{S}_{\text{eff,quad}} &= \frac{\kappa^2}{8V}\sum_{q,\mu}\widetilde{\eta}_\mu(q)\widetilde{\eta}_\mu(-q)\\ &+ \frac{1}{4}\frac{1}{V^2}\sum_{q,p}\frac{\left[\widetilde{\alpha}(q)-\hat{p}_\mu\hat{r}_\mu\widetilde{\eta}_\mu(q)\right]\left[\widetilde{\alpha}(-q)-\hat{p}_\nu\hat{r}_\nu\widetilde{\eta}_\nu(-q)\right]}{D(p)D(r)}\,,\quad r=p+q\,.\end{aligned} \tag{B.61}$$

Define ($r=p+q$):

$$H(q) = \frac{1}{V}\sum_p\frac{1}{D(p)D(r)}\,, \tag{B.62}$$

$$H_\mu(q) = \frac{1}{V}\sum_p\frac{\hat{p}_\mu\hat{r}_\mu}{D(p)D(r)}\,, \tag{B.63}$$

$$H_{\mu\nu}(q) = \frac{1}{V}\sum_p\frac{\hat{p}_\mu\hat{r}_\mu\hat{p}_\nu\hat{r}_\nu}{D(p)D(r)}\,. \tag{B.64}$$

Note all $H-$functions are even in q. Then the leading order quadratic term can be written

$$\begin{aligned}\overline{S}_{\text{eff,quad}} = \frac{1}{4}\frac{1}{V}\sum_q\Big[&\widetilde{\alpha}(q)H(q)\widetilde{\alpha}(-q) - \widetilde{\alpha}(q)H_\mu(q)\widetilde{\eta}_\mu(-q) - \widetilde{\alpha}(-q)H_\mu(q)\widetilde{\eta}_\mu(q)\\ &+\widetilde{\eta}_\mu(q)H_{\mu\nu}(q)\widetilde{\eta}_\nu(-q)\Big] + \frac{\kappa^2}{8V}\sum_{q,\mu}\widetilde{\eta}_\mu(q)\widetilde{\eta}_\mu(-q)\,.\end{aligned} \tag{B.65}$$

Defining

$$\widetilde{\beta}(q) = \widetilde{\alpha}(q) - \frac{H_\mu(q)}{H(q)}\widetilde{\eta}_\mu(q)\,, \tag{B.66}$$

[8] Here $\hat{p}_\mu = 2\sin(p_\mu/2)$.

we have diagonalized the quadratic part:

$$\overline{S}_{\text{eff,quad}} = \frac{1}{4}\frac{1}{V}\sum_q \Big[\widetilde{\beta}(q)H(q)\widetilde{\beta}(-q) + \widetilde{\eta}_\mu(q)\left\{H_{\mu\nu}(q) - \frac{H_\mu(q)H_\nu(q)}{H(q)} + \frac{1}{2}\kappa^2\delta_{\mu\nu}\right\}\widetilde{\eta}_\nu(-q)\Big]\,, \tag{B.67}$$

$$(S^{-1}TS^{-1})_{xy} = \frac{1}{V^2}\sum_{p,q}\frac{\mathrm{e}^{irx-ipy}}{D(p)D(r)}\left\{-\widetilde{\beta}(q) + X_\mu(p,q)\widetilde{\eta}_\mu(q)\right\}\,,\quad r = p+q\,, \tag{B.68}$$

where

$$X_\mu(p,q) \equiv \hat{r}_\mu\hat{p}_\mu - \frac{H_\mu(q)}{H(q)}\,,\quad r = p+q\,. \tag{B.69}$$

For the connected 4-point coupling in leading order we obtain

$$\langle \vec{e}_x\cdot\vec{e}_y\vec{e}_{x'}\cdot\vec{e}_{y'}\rangle_c = -\frac{2}{N}\frac{1}{V^3}\sum_{p,q,p'}\frac{\mathrm{e}^{ipx-iry}}{D(p)D(r)}\frac{\mathrm{e}^{ip'x'-ir'y'}}{D(p')D(r')} \times\left\{\widetilde{\triangle}(q) + X_\mu(p,q)X_\nu(p',q)\widetilde{\triangle}_{\mu\nu}(q)\right\}\,,\quad r = p+q, r' = p'-q\,, \tag{B.70}$$

where

$$\widetilde{\triangle}(q) = \frac{1}{H(q)}\,, \tag{B.71}$$

$$\widetilde{\triangle}_{\mu\rho}(q)\left\{H_{\rho\nu}(q) - \frac{H_\rho(q)H_\nu(q)}{H(q)} + \frac{1}{2}\kappa^2\delta_{\rho\nu}\right\} = \delta_{\mu\nu}\,. \tag{B.72}$$

We consider the isotropic case $T = L$, $w_0 = w_1 = w$, then in leading order for the 2- and 4-point functions:

$$\Sigma = \frac{V}{wm_0^2} + \mathcal{O}(1/N)\,, \tag{B.73}$$

$$\sum_{x,y,x',y'}\langle \vec{e}_x\cdot\vec{e}_y\vec{e}_{x'}\cdot\vec{e}_{y'}\rangle_c = -\frac{2}{N}\frac{V}{(wm_0^2)^4}\left\{\widetilde{\triangle}(0) + \frac{H_\mu(0)H_\nu(0)}{H(0)^2}\widetilde{\triangle}_{\mu\nu}(0)\right\} + \mathcal{O}(1/N^2)\,, \tag{B.74}$$

so that the renormalized coupling, eq. (5.44) is given by

$$Ng_{\mathrm{R}} = \frac{2}{w^2M^2}\left\{\widetilde{\triangle}(0) + \frac{H_\mu(0)H_\nu(0)}{H(0)^2}\widetilde{\triangle}_{\mu\nu}(0)\right\} + \mathcal{O}(1/N)\,. \tag{B.75}$$

Note (setting to this order $m_0 = M$)

$$H(0) = \frac{1}{w^2}\overline{H}_0\,, \tag{B.76}$$

$$H_\mu(0) = \frac{1}{dw^2}\overline{H}_1\,, \tag{B.77}$$

$$H_{\mu\nu}(0) = \frac{1}{w^2V}\sum_p\frac{\hat{p}_\mu^2\hat{p}_\nu^2}{(\hat{p}^2+M^2)^2} \tag{B.78}$$

$$= \frac{1}{w^2d}\left\{\overline{H}_2\delta_{\mu\nu} + \overline{H}_3\,(1-d\delta_{\mu\nu})\right\}\,, \tag{B.79}$$

where

$$\overline{H}_0 = \frac{1}{V}\sum_p \frac{1}{(\hat{p}^2+M^2)^2}\,, \tag{B.80}$$

$$\overline{H}_1 \equiv \frac{1}{V}\sum_p \frac{\hat{p}^2}{(\hat{p}^2+M^2)^2}\,, \tag{B.81}$$

$$\overline{H}_2 \equiv \frac{1}{V}\sum_p \frac{(\hat{p}^2)^2}{(\hat{p}^2+M^2)^2}\,, \tag{B.82}$$

$$\overline{H}_3 \equiv \frac{1}{(d-1)V}\sum_p \frac{(\hat{p}^2)^2-\hat{p}^4}{(\hat{p}^2+M^2)^2}\,, \tag{B.83}$$

where

$$\hat{p}^r \equiv \sum_\mu \hat{p}_\mu^r\,. \tag{B.84}$$

Then

$$\widetilde{\triangle}_{\mu\nu}(0) = \frac{w^2}{\frac{1}{2}\kappa^2 d w^2 + \overline{H}_2 - d\overline{H}_3}\{d\delta_{\mu\nu}-1\} + \frac{w^2}{\left[\frac{1}{2}\kappa^2 d w^2 + \overline{H}_2 - \overline{H}_1^2/\overline{H}_0\right]}\,, \tag{B.85}$$

and so

$$\widetilde{\triangle}(0) + \frac{H_\mu(0)H_\nu(0)}{H(0)^2}\widetilde{\triangle}_{\mu\nu}(0) = \frac{w^2}{\overline{H}_0} + \frac{w^2\overline{H}_1^2}{\overline{H}_0^2\left[\frac{1}{2}\kappa^2 d w^2 + \overline{H}_2 - \overline{H}_1^2/\overline{H}_0\right]}\,. \tag{B.86}$$

Noting

$$\overline{H}_1 = w - M^2\overline{H}_0\,, \tag{B.87}$$

$$\overline{H}_2 = 1 - 2wM^2 + M^4\overline{H}_0\,, \tag{B.88}$$

we get

$$N g_{\rm R} = \frac{2}{M^2\overline{H}_0} + \frac{2\left(M^2\overline{H}_0 - w\right)^2}{M^2\overline{H}_0^2\left[1+\frac{1}{2}d\kappa^2 w^2 - w^2/\overline{H}_0\right]} + \mathcal{O}(1/N)\,. \tag{B.89}$$

B.2.2 Lattice artifacts

In the rest of this section we restrict attention to $d = 2$ and consider large physical volumes.

To see the structure of artifacts we expand w and $\overline{H}_0$:

$$w = \frac{1}{4\pi}\mathcal{L} + \frac{M^2}{32\pi}(1-\mathcal{L}) + \ldots\,, \tag{B.90}$$

$$M^2\overline{H}_0 = \frac{1}{4\pi} - \frac{M^2}{32\pi}(2-\mathcal{L})\ldots\,, \tag{B.91}$$

where $\mathcal{L} = -\ln(M^2/32)$.

Taking the continuum limit we have $\kappa^2 w^2 = q^2 + \mathcal{O}(1/L^2)$, with q given by eq. (5.41). Using eqs. (B.90), (B.91) in eq. (B.89) (with $d = 2$) we derive eq. (5.47).

B.2.3 Numerical evaluation of $g_{\rm R}$

In the infinite volume limit the gap equations are

$$J(M) = w\,, \tag{B.92}$$

and

$$\kappa^2\left(w - \frac{1}{f}\right) + M^2 = \frac{1}{w}\,, \tag{B.93}$$

where

$$J(M) = \int_{-\pi}^{\pi} \frac{\mathrm{d}^2 p}{(2\pi)^2} \frac{1}{K(p) + M^2} = \int_{-\pi}^{\pi} \frac{\mathrm{d}p}{2\pi} \frac{1}{\sqrt{\omega(\omega+4)}}\,. \tag{B.94}$$

Inserting $w = J(M)$ into eq. (B.92) one can find numerically $M = M(f, \kappa)$.

One also has

$$\overline{H}_0(M) = \int_{-\pi}^{\pi} \frac{\mathrm{d}^2 p}{(2\pi)^2} \frac{1}{\left(K(p) + M^2\right)^2} = \int_{-\pi}^{\pi} \frac{\mathrm{d}p}{2\pi} \frac{\omega + 2}{\left[\omega(\omega+4)\right]^{3/2}}\,. \tag{B.95}$$

Inserting these expressions into eq. (B.89) it is easy to calculate $N g_{\rm R}(aM)$.

References

[1] A. B. Zamolodchikov and A. B. Zamolodchikov, *Factorized S Matrices in Two-Dimensions as the Exact Solutions of Certain Relativistic Quantum Field Models*, *Annals Phys.* **120** (1979) 253.

[2] A. M. Polyakov and P. B. Wiegmann, *Theory of Nonabelian Goldstone Bosons*, *Phys. Lett. B* **131** (1983) 121.

[3] P. B. Wiegmann, *Exact Solution Of The O(3) Nonlinear Sigma Model*, *Phys. Lett. B* **152** (1985) 209.

[4] P. Hasenfratz, M. Maggiore and F. Niedermayer, *The Exact mass gap of the O(3) and O(4) nonlinear sigma models in d = 2*, *Phys. Lett. B* **245** (1990) 522.

[5] J. Balog and A. Hegedüs, *TBA Equations for excited states in the O(3) and O(4) nonlinear sigma model*, *J. Phys. A* **37** (2004) 1881 [hep-th/0309009].

[6] A. Hegedüs, *Nonlinear integral equations for finite volume excited state energies of the O(3) and O(4) nonlinear sigma-models*, *J. Phys. A* **38** (2005) 5345 [hep-th/0412125].

[7] J. Balog and A. Hegedüs, *TBA equations for the mass gap in the O(2r) non-linear sigma-models*, *Nucl. Phys. B* **725** (2005) 531 [hep-th/0504186].

[8] J. Balog and A. Hegedüs, *The finite size spectrum of the 2-dimensional O(3) nonlinear sigma-model*, *Nucl. Phys. B* **829** (2010) 425 [arXiv:0907.1759 [hep-th]].

[9] M. Lüscher, P. Weisz and U. Wolff, *A Numerical method to compute the running coupling in asymptotically free theories*, *Nucl. Phys. B* **359** (1991) 221.

[10] U. Wolff, *Collective Monte Carlo Updating for Spin Systems*, *Phys. Rev. Lett.* **62** (1989) 361.

[11] U. Wolff, *Asymptotic Freedom And Mass Generation In The O(3) Nonlinear Sigma Model*, *Nucl. Phys. B* **334** (1990) 581.

[12] K. Symanzik, *Continuum Limit and Improved Action in Lattice Theories. 1. Principles and phi**4 Theory*, *Nucl. Phys. B* **226** (1983) 187.

[13] K. Symanzik, *Continuum Limit and Improved Action in Lattice Theories. 2. O(N) Nonlinear Sigma Model in Perturbation Theory*, *Nucl. Phys. B* **226** (1983) 205.

[14] M. Lüscher and P. Weisz, *On-Shell Improved Lattice Gauge Theories*, *Commun. Math. Phys.* **97** (1985) 59 [*Erratum ibid.* **98** (1985) 433].

[15] M. Lüscher and P. Weisz, *Computation of the Action for On-Shell Improved Lattice Gauge Theories at Weak Coupling*, *Phys. Lett. B* **158** (1985) 250.

[16] M. Hasenbusch, P. Hasenfratz, F. Niedermayer, B. Seefeld and U. Wolff, *Nonstandard cutoff effects in the nonlinear sigma model*, *Nucl. Phys. Proc. Suppl.* **106** (2002) 911 [hep-lat/0110202].

[17] F. Knechtli, B. Leder and U. Wolff, *Cutoff effects in O(N) nonlinear sigma models*, *Nucl. Phys. B* **726** (2005) 421 [hep-lat/0506010].

[18] J. Balog, F. Niedermayer and P. Weisz, *Logarithmic corrections to O(a**2) lattice artifacts*, *Phys. Lett. B* **676** (2009) 188 [arXiv:0901.4033 [hep-lat]].

[19] P. Hasenfratz and F. Niedermayer, *Perfect lattice action for asymptotically free theories*, *Nucl. Phys. B* **414** (1994) 785 [hep-lat/9308004].

[20] W. Bietenholz, U. Gerber, M. Pepe and U. -J. Wiese, *Topological Lattice Actions*, *JHEP* **1012** (2010) 020 [arXiv:1009.2146 [hep-lat]].

[21] M. Lüscher, *Topology of Lattice Gauge Fields*, *Commun. Math. Phys.* **85** (1982) 39.

[22] A. Patrascioiu and E. Seiler, *Phase structure of two-dimensional spin models and percolation*, *J. Statist. Phys.* **69** (1992) 573.

[23] A. Patrascioiu and E. Seiler, *Percolation theory and the existence of a soft phase in 2-D spin models*, *Nucl. Phys. Proc. Suppl.* **30** (1993) 184.

[24] M. Aizenman, *On the slow decay of O(2) correlations in the absence of topological excitations: remark on the Patrascioiu-Seiler model*, *J. Stat. Phys.* **77** (1994) 351.

[25] W. Bietenholz, A. Pochinsky and U. J. Wiese, *Meron cluster simulation of the theta vacuum in the 2-d O(3) model*, *Phys. Rev. Lett.* **75** (1995) 4524 [hep-lat/9505019].

[26] M. Hasenbusch, *O(N) and RP**(N-1) models in two-dimensions*, *Phys. Rev. D* **53** (1996) 3445 [hep-lat/9507008].

[27] P. Hernandez, K. Jansen and M. Lüscher, *Locality properties of Neuberger's lattice Dirac operator*, *Nucl. Phys. B* **552** (1999) 363 [hep-lat/9808010].

[28] M. Lüscher, *Abelian chiral gauge theories on the lattice with exact gauge invariance*, *Nucl. Phys. B* **549** (1999) 295 [hep-lat/9811032].

[29] M. Lüscher, *Weyl fermions on the lattice and the nonAbelian gauge anomaly*, *Nucl. Phys. B* **568** (2000) 162 [hep-lat/9904009].

[30] A. Patrascioiu and E. Seiler, *Percolation and the existence of a soft phase in the classical Heisenberg model*, *J. Statist. Phys.* **106** (2002) 811 [hep-th/0011199].

[31] H. Fukaya and T. Onogi, *Lattice study of the massive Schwinger model with theta term under Luscher's 'admissibility' condition*, *Phys. Rev. D* **68** (2003) 074503 [hep-lat/0305004].

[32] H. Fukaya and T. Onogi, *Theta vacuum effects on the chiral condensation and the eta-prime meson correlators in the two flavor massive QED(2) on the lattice*, *Phys. Rev. D* **70** (2004) 054508 [hep-lat/0403024].

[33] H. Fukaya, S. Hashimoto, T. Hirohashi, K. Ogawa and T. Onogi, *Topology conserving gauge action and the overlap-Dirac operator*, *Phys. Rev. D* **73** (2006) 014503 [hep-lat/0510116].

[34] W. Bietenholz, K. Jansen, K. -I. Nagai, S. Necco, L. Scorzato and S. Shcheredin, *Exploring topology conserving gauge actions for lattice QCD*, *JHEP* **0603** (2006) 017 [hep-lat/0511016].

[35] M. Bögli, F. Niedermayer, M. Pepe and U. J. Wiese, *Non-trivial theta-Vacuum Effects in the 2-d O(3) Model*, *JHEP* **1204** (2012) 117 [arXiv:1112.1873 [hep-lat]].

[36] D. Nogradi, *An ideal toy model for confining, walking and conformal gauge theories: the O(3) sigma model with theta-term*, *JHEP* **1205** (2012) 089 [arXiv:1202.4616 [hep-lat]].

[37] D. Controzzi and G. Mussardo, *On the mass spectrum of the two-dimensional O(3) sigma model with theta term*, *Phys. Rev. Lett.* **92** (2004) 021601 [hep-th/0307143].

[38] B. Alles and A. Papa, *Numerical study of the mass spectrum in the 2D O(3) sigma model with a theta term*, *PoS LAT* **2007** (2007) 287 [arXiv:0711.1803 [hep-lat]].

[39] B. Berg and M. Lüscher, *Definition and Statistical Distributions of a Topological Number in the Lattice O(3) Sigma Model*, *Nucl. Phys. B* **190** (1981) 412.

[40] J. Balog, F. Niedermayer and P. Weisz, *The Puzzle of apparent linear lattice artifacts in the 2d non-linear sigma-model and Symanzik's solution*, *Nucl. Phys. B* **824** (2010) 563 [arXiv:0905.1730 [hep-lat]].

[41] J. Balog, *to be published.*

[42] J. Balog, M. Niedermaier, F. Niedermayer, A. Patrascioiu, E. Seiler and P. Weisz, *The intrinsic coupling in integrable quantum field theories*, *Nucl. Phys. B* **583** (2000) 614 [hep-th/0001097].

[43] M. Lüscher, *A New Method to Compute the Spectrum of Low Lying States in Massless Asymptotically Free Field Theories*, *Phys. Lett. B* **118** (1982) 391.

[44] S. Caracciolo and A. Pelissetto, *Corrections to finite-size scaling in the lattice N-vector model for N = infinity*, *Phys. Rev. D* **58** (1998) 105007 [hep-lat/9804001].